

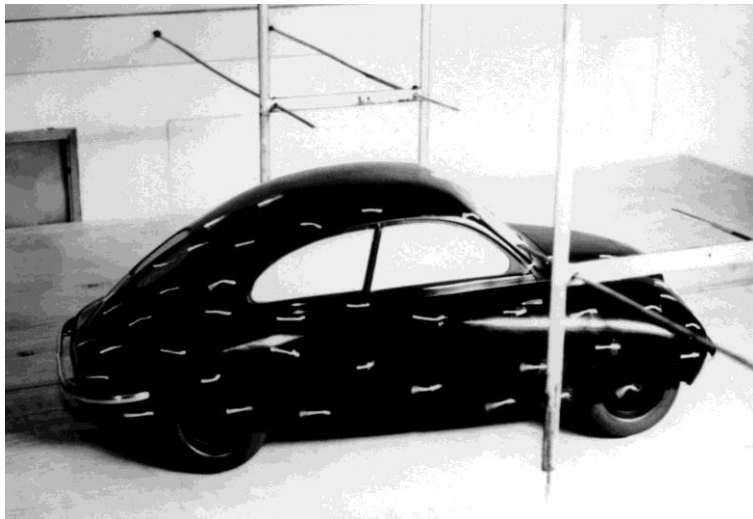
THESIS FOR THE DEGREE OF DOCTOR OF PHILOSOPHY

in

MACHINE AND VEHICLE SYSTEMS

Under-body and Diffuser Flows of Passenger Vehicles

JESPER MARKLUND



Department of Applied Mechanics
CHALMERS UNIVERSITY OF TECHNOLOGY
Gothenburg, Sweden, 2013

Under-body and Diffuser Flows of Passenger Vehicles

The influence of vehicle rear under-body design on the total drag coefficient

JESPER MARKLUND

ISBN 978-91-7385-866-3

© **JESPER MARKLUND, 2013**

Doktorsavhandlingar vid Chalmers tekniska högskola

Ny serie nr 3547

ISSN: 0346-718X

Department of Applied Mechanics

Chalmers University of Technology

SE-412 96 Gothenburg

Sweden

Telephone +46 (0)31 7721000

Cover:

Ursaab in a wind tunnel, 1947. (Courtesy of SAAB Car Museum).

Chalmers Reproservice

Gothenburg, Sweden 2013

Under-body and Diffuser Flows of Passenger Vehicles

Jesper Marklund
Department of Applied Mechanics
Chalmers University of Technology

Abstract

Energy efficient vehicles will be required to meet future emission and fuel consumption requirements. Customers require reduced fuel consumption due to increasing fuel prices and the environmental issues, are drivers to reduce CO₂. It is essential to improve the drivelines, but improving resistance forces of the vehicle is also an efficient and sustainable way to improve energy efficiency. Aerodynamic drag is the dominating resistance force for passenger and commercial vehicles at highway speeds.

A passenger car is a bluff body aerodynamically, with pressure forces at the rear that dominate the aerodynamic drag. This is due to a relatively square shape, with a length / height ratio of approximately three, and a truncated rear-end that generates a wake. About 60 % of the aerodynamic drag forces of a passenger vehicle are related to the exterior body, upper and under-body; the rest being related to wheel, wheel house and cooling drag.

This work focuses on the aerodynamics of the rear-end and under-body of bluff bodies in general, but also applied to passenger cars. Firstly, simplified bluff bodies, that represent different vehicle types, were used to study and map the general behaviour of the bodies. The findings were then tested and applied to full-size vehicles, with the focus on under-body flows and the effect of under-body diffusers. Both experimental and numerical tools were used, and scale model as well as full-size test bodies have been investigated.

A unique feature with road vehicle aerodynamics are the boundary conditions: ground proximity and moving ground; relative the body. Also, rotating wheels and a cooling flow that re-distributes the flow around the body have to be considered. The Chalmers L2 wind tunnel is equipped with a moving ground system, and the simulations were set up with moving ground, rotating wheels and a cooling flow. The rotating wheels were simulated with the MRF approach and the cooling flow was tuned by measuring the cooling flow of a full-sized car and using this data in the simulations.

A significant difference in the flow in an under-body diffuser, depending on upper body, was noticed in the bluff body experiments. In particular, drag was reduced more for a sedan or fastback upper body, compare to a wagon or square-back. This difference was confirmed in simulations of full-size vehicles, under road-vehicle boundary conditions, with under-body diffusers applied. It was found that it is very important to have flow symmetry around the vehicle and especially at the wake, to optimize pressure recovery at the rear end and reduce drag.

Keywords: Vehicle aerodynamics, Bluff bodies, CFD, Wake flow, Boundary layer

List of papers

This thesis is based on the work presented in the following appended papers.

- I. Marklund J. Löfdahl L. Influence of a Diffuser To The Wake Flow of a Passenger Car, ASME Summer Meeting FESM2012, 8-12 July 2012, Rio Grande, Puerto Rico, USA.
- II. Marklund, J., Lofdahl, L., Danielsson, H. and Olsson, G., "Performance of an Automotive Under-Body Diffuser Applied to a Sedan and a Wagon Vehicle," *SAE Int. J. Passeng. Cars - Mech. Syst.* 6(1):2013, doi:10.4271/2013-01-0952.
- III. Marklund, J., Lofdahl, L., "The Influence of Ground Proximity on the Flow Field around Different Bluff Bodies", Submitted to Journal of Fluids Engineering.
- IV. Marklund, J., Lofdahl, L., "Effect of an Under-body Diffuser to the Aerodynamic Performance of Sedan and Wagon Type Cars", Submitted to Journal of Fluids Engineering.

Done by the author

The author has produced all the test results and written all the manuscripts. Co-authors have provided input such as discussing input, revising manuscripts and administrative support. Simulation work in paper II and paper III was carried out by the author with help from J. Zaya at Chalmers.

Other relevant publications by the author

- Marklund J. Löfdahl L. Wake Measurement of a Simple Bluff Body With Varying Rear End Design and Close Proximity to Ground, ASME Summer Meeting FESM2010, 1-5 August 2010, Montreal, CANADA.
- Marklund J. Löfdahl L. Flow Field Around and in a SAAB 9-3 Convertible, Euromech Colloquium 509, Berlin, Germany 24-25 March 2009.
- Marklund J. Löfdahl L. Drag and Lift Measurements of Four Bluff Bodies, Collaborative Report, GM Research and Development Center, May 2010.
- Marklund J. Löfdahl L. Aerodynamics of passenger vehicles – Bluff Bodies, The Vehicle Component, Article SVEN, Issue 1, 2012.

Acknowledgement

This work would not have been possible without the support from a lot of people. First of all my supervisors, Mr. Håkan Danielsson at former Saab Automobile AB and Professor Lennart Löfdahl at Chalmers University of Technology. Lately also Gunnar Olsson from LeanNova Engineering for supporting and leading this project as a project leader. Without their support this job would never have been possible.

A special thanks to all former colleagues at Saab Aerodynamics Department , including Simulation Group, for help and co-work during this project. The situation at Saab Automobile has been extreme for the last years and it is a unique experience that has been shared among the staff. It is amazing to see the enthusiasm and loyalty that has been spread around all the Saab employees during the difficult times. Everybody has moved on to other employment to meet new challenges.

At Chalmers University of Technology Alexey Vdovin helped a lot with computer related issues and Johan Zaya for help with simulation work. Thanks Lisa Larsson, Helena Martini and Jonathan Rice for being good colleagues and daily discussions.

To the former members of Vehicle Aerodynamic Group at Chalmers, Dr. Christoffer Landström for good friendship, all the help in the lab plus all kinds of Matlab issues. Dr. David Söderblom, and Dr. Peter Gullberg for support and good friendship. Also thank you Andrew Dawkes at Chalmers for help with manufacturing of hardware, test models and proof reading this manuscript.

Furthermore, I am grateful for the financial support from the Swedish Energy Agency as funder of this project. I appreciate the support from former Saab Automobile and now Combitech AB for funding and owning the project. Chalmers Computational Center for Science and Engineering (C3SE) and the Swedish National Infrastructure for Computing (SNIC) for providing computational resources.

Finally also family and friends for continuous help and support.

Göteborg, 2013.
Jesper Marklund

Nomenclature

A	Projected front area	$[m^2]$
m	Mass of vehicle	$[kg]$
p	Pressure	$[Pa]$
g	Gravity	$[m/s^2]$
F_D	Aerodynamic drag force	$[N]$
F_a	Acceleration force	$[N]$
F_R	Rolling resistance force	$[N]$
F_x	Tractive force	$[N]$
F_G	Driving force due to gravity	$[N]$
ρ	Fluid density	$[kg/m^3]$
ν	Kinematic viscosity	$[m^2/s]$
α	Road inclination	$[deg]$
U_∞	Free stream velocity	$[m/s]$
u	Velocity	$[m/s]$
t	Time	$[s]$
T	Temperature	$[K]$
L	Length	$[m]$
W	Width	$[m]$
C_D	Drag coefficient	$[-]$
C_L	Lift coefficient	$[-]$
C_p	Pressure coefficient	$[-]$
C_{pd}	Diffuser pressure recovery constant	$[-]$
Re	Reynolds number	$[-]$
f_r	Rolling resistance coefficient	$[-]$
y^+	Non-dimensional wall distance	$[-]$

Abbreviations

RANS	Reynolds Averaged Navier Stokes
CPU	Central Processing Unit
CFD	Computational Fluid Dynamics
LES	Large Eddy Simulation
MRF	Multiple Reference Frame
EPA	Environmental Protection Agency
NHTSA	National Highway Traffic Safety Administration
EU	European Union
CAC	Charge Air Cooler
SAE	Society of Automotive Engineers
ASME	American Society of Mechanical Engineers
NASA	National Aeronautical Space Administration
NACA	National Advisory Committee for Aeronautics
OEM	Original Equipment Manufacturer

ICE	Internal Combustion Engine
FEV	Full Electric Vehicle
CRFM	Condenser Radiator and Fan Module
CAFE	Corporate Average Fuel Economy

Table of Content

1.	Introduction.....	3
1.1.	Background.....	6
1.2.	Objectives	6
2.	Vehicle Aerodynamics.....	7
2.1.	Bluff and Slender Bodies.....	7
2.2.	Aerodynamics of Passenger Cars	10
2.3.	Aerodynamic optimization of passenger cars.....	13
2.4.	Diffuser of a passenger car	15
2.5.	Aerodynamic devices	17
2.5.1	NACA ducts	17
2.6.	Partial drag.....	18
3.	Method	19
3.1.	Experimental method.....	19
3.1.1	The wind tunnel.....	19
3.1.2	The test models.....	20
3.1.3	Force measurements	22
3.1.4	Pressure measurements	22
3.2.	Numerical method	25
3.2.1	RANS	25
3.2.2	CFD approach	26
3.2.3	Boundary conditions	26
3.2.4	Simplified models	27
3.2.5	Vehicle models.....	27
3.3.	Comparing CFD and measurements.....	29
4.	Results.....	31
4.1.	Characteristics of bluff body rear end models.....	31
4.2.	Passenger vehicle applications	44
4.2.1	Energy usage	52
5.	Concluding remarks	55
6.	Future outlook.....	56
7.	Summary of papers	57
8.	References.....	59

1. Introduction

Increased fuel prices and environmental issues are the biggest incentives for reducing the fuel consumption of passenger vehicles. With increased wealth the demand for personal transportation grows and the need of road, sea, and air transport increases. The production of cars has continually increased over the past 15 years, but commercial vehicles have been more constant. The financial crisis starting in 2008 and the concurrent increase in oil price made a strong impact on society and vehicle production decreased. A plot of production statistics for the past 15 years, Figure 1 shows that the market has regained the losses and continues to grow again.

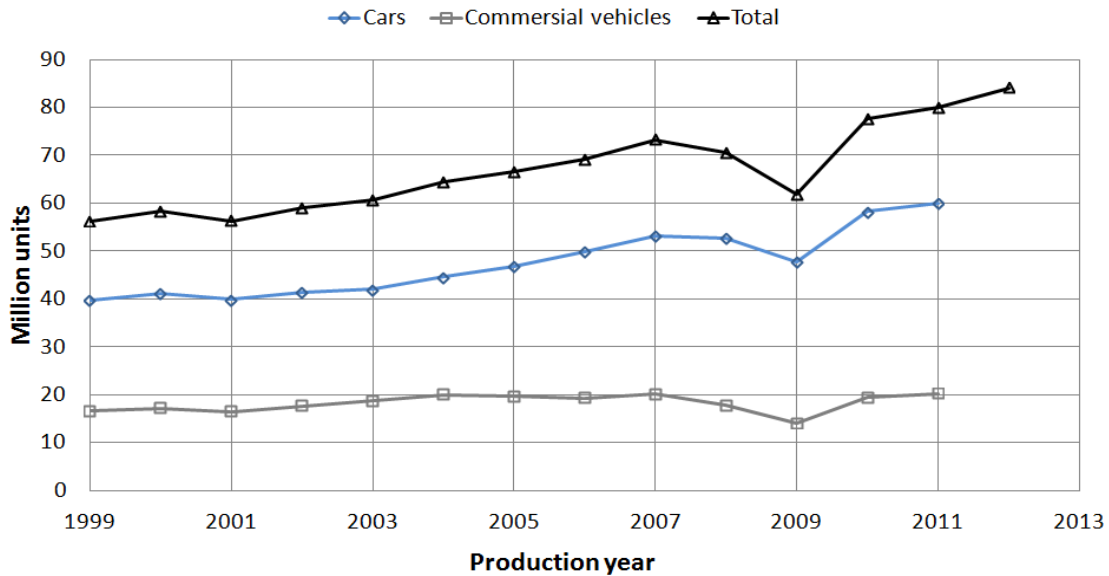


Figure 1 Statistics of vehicle production from OICA [1].

At the time of writing, China is the largest manufacturer of cars and responsible for the long term growth, followed by India. The increase for China was 6% in 2012 and has slowed down from previous years. Other regions have been constant or decreased over this period. North American production increased 17% last year and in Europe the fall continued. Europe has a large part of car production with 26% of total production in 2011, and North America has a large part of the commercial vehicle production with 39%. This is partly due to a large percentage of light trucks that are defined as commercial vehicle in the statistics. Sales do not always follow the production statistics, but Asia was the largest market with 42%, followed by North and South America 28% and Europe 21% in 2011 [2]. OICA estimates that sales of vehicles will grow 3% during 2013 due to good forecasts in China and USA.

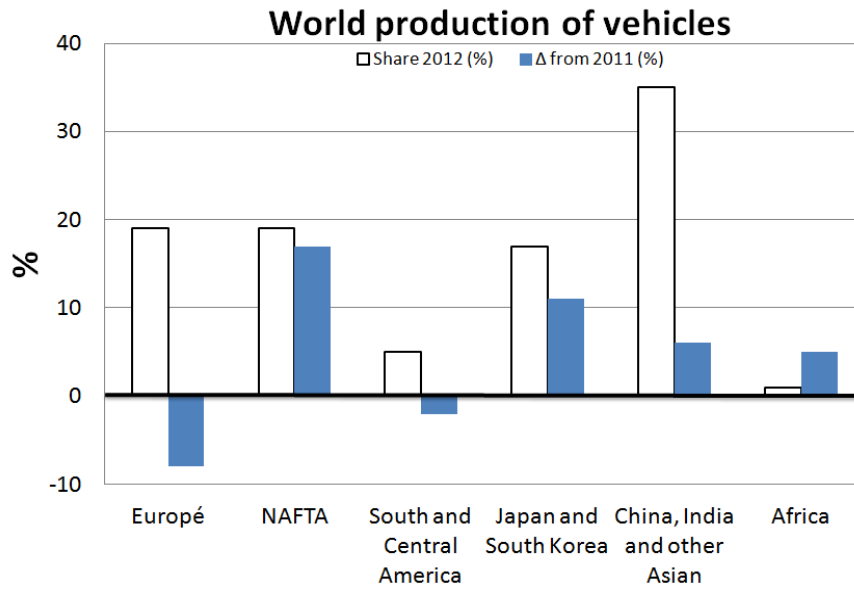


Figure 2 Regional vehicle production in 2012 and the change from 2011 [1].

Global energy consumption grew 2.5% in 2011 and the primary fuels were, Oil 33.1%, coal 30.3% and natural gas approximately 30% [3]. Exxon Mobile concludes in their energy outlook for 2040 that energy demand in developing countries will increase 65% due to growing prosperity and growing economies. Growth will come in the demand for electricity and the transport sector. The number of cars are predicted to double by 2040, and the total transport sector, car, truck, planes, ships and trains will increase 40% [4]. Germany has announced their intention to close their nuclear power plants by 2030, and Japan has said their intention is to close all nuclear power plants by 2040 [5]. Public opinion in Japan has changed after the Fukushima accident even though nuclear power represents 30% of total energy usage. The intention being to replace it with renewable energy both in Japan and Germany. These two together has applied pressure for new efficient technology, so that deficiency will not be replaced with fossil fuel. Global road transport is responsible for approximately 16% of the man-made CO₂ emissions [1], so to make a significant change, the problems must be more widely addressed. As the vehicle industry is still a significant proportion, the pressure for more energy-efficient vehicles is large.

There are many challenges to developing sustainable mobility. The most sustainable way is to reduce resistance forces needed to move the vehicles by improved technique and minimal losses during the transport. For CO₂ reduction the propulsion system must also be improved and preferably replaced by other technologies than the combustion of fossil fuel. This is partly done by hybrid and fully electric vehicles, but a sustainable solution also requires that the total energy consumption is reduced. It is important that the source of electricity is not produced with fossil fuel, and to have an efficient battery technology that is re-usable. It is also important to reduce power needed for accessories such as air condition system, power steering and electrical systems because that is a substantial part of parasitic drag of the vehicle.

The energy density in diesel fuel is 11.85 kWh/kg and energy storage in a battery is 0.029-0.265 kWh/kg (lead - Li-Ion). The best rechargeable batteries for energy storage

are Lithium Ion and Lithium Polymer [6]. The energy density in diesel is 45-60 times the energy in batteries. The volumetric ratio is better for batteries due to its higher density compared to the liquids. Density of diesel (according to EN590) is 0.84kg/l and for gasoline (with 5% ethanol) it is 0.752kg/l, which means that the same volume of diesel contains almost 10% more energy than gasoline. A graph of energy density of selected batteries and diesel/gasoline is shown in Figure 3.

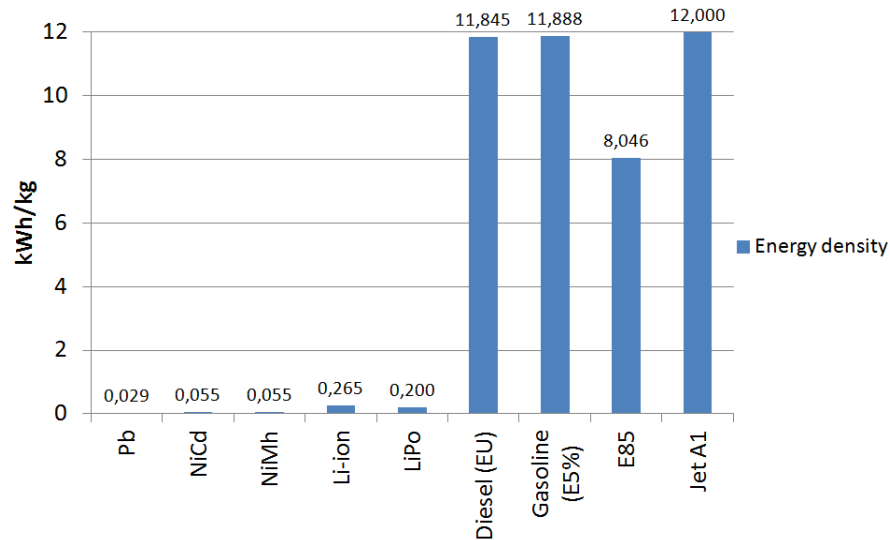


Figure 3 Energy density of electric batteries compared to diesel and gasoline [7].

The efficiency of an electric motor is 85-90% but for a diesel engine around 40%. Thus the usable energy in Lithium-Ion batteries is 5% of diesel fuel, or that the same amount of energy in batteries would have 20 times the mass of diesel. This has a large impact on vehicle resistance forces and would require even more energy for propulsion. Currently it is not possible for an electrical vehicle to have the same performance as an ICE vehicle and still have the same range with the available battery technology. Tesla cars [8] use Lithium-Ion battery technology and offer a full electric sport vehicle with a power of 215kW a mass of 1235kg and a range of 400km. Battery energy density is claimed to be 174Wh/kg.

The method of specifying the CO₂ target to the vehicle manufacturers used today, is an average emission value for the complete fleet of cars sold, by the manufacturer. In Europe this is regulated by the EC regulation and in the USA by the CAFE standard. The cars are tested in defined test cycles and in Europe that is the NEDC (New European Driving Cycle) [9]. The new CO₂ requirement for Europe from 2020 is 95g CO₂/100km and there are penalties defined for not fulfilling them. If the vehicle manufacturer sells full-electric vehicles with zero emissions, the average CO₂ emissions of the fleet will be reduced. Many car manufacturers have started to provide full-electric vehicles and the main challenges are sufficient range and high purchase price of the vehicles.

There is no doubt that future CO₂ emission requirements will be very challenging for the vehicle manufacturers in EU and in the USA. Europe has already taken a large step by moving towards energy-efficient diesel cars. Improving the aerodynamics of a vehicle gives a direct reduction of the vehicle resistance and will be one method to reduce

CO₂ emissions. More changes, especially to the drivelines, must also be made to reach these new targets.

1.1. Background

It is well known by all vehicle manufacturers that legislation will require a reduction of the CO₂ emissions in the near future. It is also a fact that customer demands will require reduced fuel consumption because of increased fuel prices. Figure 4 shows the rolling resistance, and the aerodynamic resistance relative to vehicle speed. The vehicle is a generic passenger car with a mass of 1600kg, front area of 2.2m² and a C_D of 0.30. The rolling resistance is nearly linear, and at 60-80 km/h the aerodynamic drag will be the dominant resistance force due to its increase by the square of vehicle speed. Acceleration in normal city driving is typically around 1m/s² and in the NEDC the accelerations are specified to this magnitude or less. The resistance force from the inertia will be peak loads and depending on mass of the vehicle. It is a force to be overcome during positive acceleration, and it is a force that can be regained if the vehicle is equipped with a brake regeneration system. The line 1m/s² acceleration also represent the force required to drive the same vehicle uphill in a 9.8% slope.

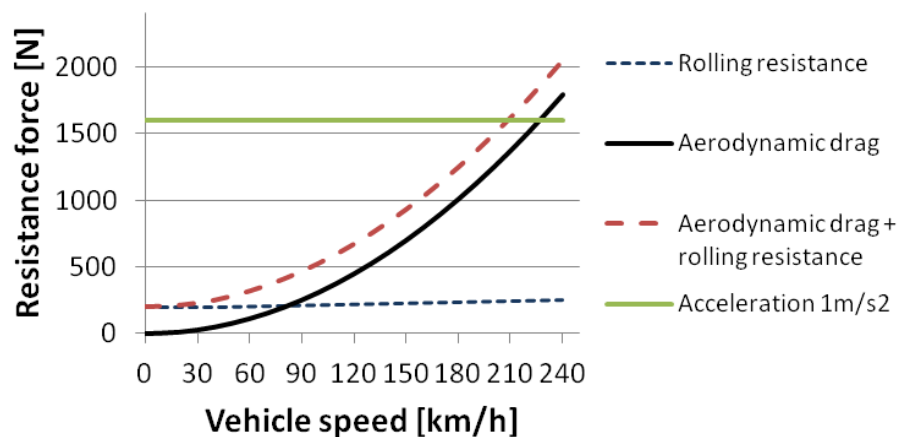


Figure 4 Plot of resistance forces for a generic passenger car at constant speed and on level road, versus vehicle speed.

Improving the aerodynamic drag is important because it is the single biggest driving resistance at higher speeds, and new techniques can be effective at a relatively low cost. The key areas are the exterior body shape, the under-body and the wheelhouse airflows; but also the cooling air flows have significant effects on drag.

1.2. Objectives

This project focuses on the rear part of the exterior body and under-body. The objectives were to understand the flow field in the close wake and to be able to use the knowledge to reduce the drag of the vehicle. This meant knowing how to design the rear end, including the under-body, for low-drag under road-vehicle boundary conditions such as ground proximity, rotating wheels and moving ground. The goal was to understand what parameters are important and how to use them for a design of low-drag passenger cars.

2. Vehicle Aerodynamics

There are many aerodynamic properties that affect a passenger car besides the performance effect such as fuel consumption. Lift and side-forces are important to the stability and safety of the vehicle, and have a major effect on directional stability and cross-wind sensitivity. Wind noise and contamination are comfort issues, and cooling of components are function-related properties. All requirements have to be considered in the design process of a passenger car and in the end it will be a compromise between styling and the many functional parameters. Lately the focus on reducing fuel consumption and CO₂-emissions has increased the importance of aerodynamic drag. More than half of the drag originates from the exterior body and under-body, and the rest is related to the wheels and cooling flows. As stated earlier the most important part in this work is to reduce drag of the vehicle focusing on the exterior body and under-body.

2.1. Bluff and Slender Bodies

The Reynolds number is a ratio of the inertia forces and the viscous forces. It can also be interpreted as the ratio of the pressure and shear force that act on the body according to Eq. (1) [10]. Viscosity is due to the molecular friction between the fluid particles. The shear stress is proportional to the velocity gradient close to the surface, $\tau = \mu(\delta u/\delta y)$.

$$\frac{\text{Pressure forces}}{\text{Shear forces}} = \frac{p - p_{\infty}}{\tau} \sim \frac{\rho u^2}{\mu \frac{\partial u}{\partial y}} \sim \frac{\rho U^2}{\mu \frac{U}{L}} \sim \frac{\rho UL}{\mu} = R_e \quad (1)$$

$$R_e = \frac{\rho UL}{\mu} = \frac{UL}{\nu} \quad (2)$$

$\nu = \mu/\rho$ is the kinematic viscosity of the fluid. If the Reynolds number increases, the pressure forces, or air speed, will be more important, and consequently the viscous effects become less important. The higher the Reynolds number is, the thinner the boundary layer will be, relative to the body. A thinner boundary layer makes the flow behave more as inviscid flow. When the Reynolds number is large enough the lift forces and moments will be Reynolds number independent i.e. independent of viscosity. Drag will not be Reynolds number independent. This assumption is only valid for streamlined bodies that are aligned with the free-stream flow. For bluff bodies with a large rear face and separated flows the forces and moments are always related to the viscosity. Separated flow is when the boundary layer detaches from the surface and creates a wake behind the body.

The drag force can be divided into friction drag and pressure drag. The friction drag comes from the friction between the fluid and the surface of the body and will be the sum of the shear forces in the fluid, as discussed above. This will appear in the boundary layer and be dominant for slender bodies. Friction drag is important for attached flows and is related to the surface area it affects. Pressure drag is due to the wakes and vortices

in the flow and will be the sum of forces acting normal to all the surfaces. Pressure drag is dominating for separated flows and is related to the surface area of the model in flow direction. A model is called streamlined, or slender, when the friction drag is dominating, and is called bluff when the pressure drag is dominating [11]. A streamlined model will always have lower drag than a bluff body of the same size [12]. Illustrations of bluff body and streamlined body with the same drag force can be seen in Figure 5.

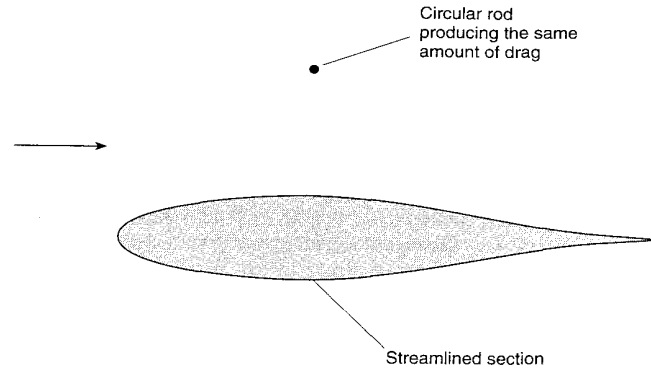


Figure 5 Comparison of streamlined body and circular rod with the same drag force [13].

Most of the pressure drag of a bluff body is generated at the rear end. When the flow separate at the rear end it will leave a large wake that generate a low pressure over a large base area. A body such as a passenger car in full scale, with a length/height ratio of about 3 and sharp corner radius, generally has a small dependency of Reynolds number. But for rounded rear end shapes the separation is not fixed in time and the boundary layer separation may vary with Reynolds number. This generates side, lift and drag forces that are time dependant and create instability in the flow. This is not desired for passenger cars and for this reason big radiuses at the rear end should be avoided. In the front, radius should be large enough to provide attached flow independent of Reynolds number.

Drag has a dependency to the lift forces of the body. The pressure difference of the low pressure areas, such as backlight of a fastback car, generates longitudinal vortices. With the starting point that the induced drag, from wing theory is defined as:

$$C_{DI} = K_V C_L^2 \quad (3)$$

where C_L is the lift coefficient and K_V is a vortex drag factor. K_V is approximately given by $k(\pi AR)^{-1}$, where AR is the aspect ratio and is defined as b^2/S , where b is the span and S is the wing plan area.

A parabolic relationship between lift and drag is clear, with an optimum drag in relation to lift, the conclusion being that the vortex component gives this relation. The vortex drag factor, K_v , reduces with reduced ground clearance and even more with a moving ground. The vortex drag factor is heavily dependent on the body width and is also a function of the body bluntness.

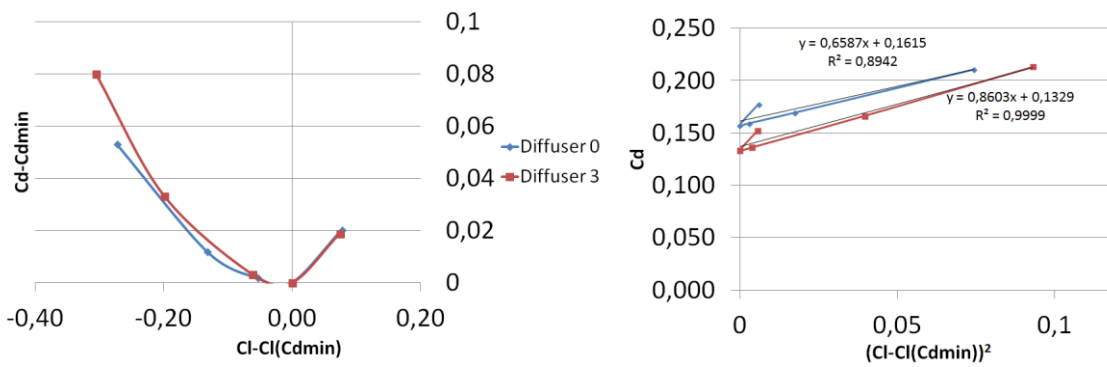


Figure 6 Drag and lift relationship depending on backlight angle, for two different diffuser angles. Left: C_D to C_L relationship. Right: C_D to C_L^2 relationship.

The relationship between drag and lift from bluff body measurements [14] is plotted in Figure 6. The backlight angle varied from 0° to 21° and it was tested for two different diffuser angles of 0° and 3° . Drag is normalized with drag minimum and lift is normalized with lift at the same point to make the curves pass origo. Drag reduces in a parabolic curve relative to lift until 15° backlight angle, and then increases again for larger backlight angles. The drag reduction is linear relative to C_L^2 until 15° backlight angle. Higher backlight angles increase drag but the relationship to C_L^2 is lost and C_D increases more relative to C_L^2 . The drag is no longer vortex induced since there is separated flow at the backlight. Similar results were found by Howell et al. [15][16] were there was also found to be a dependence on the aspect ratio of the backlight. Wickern et al. performed a study [17] of drag/lift ratio, from vortex induced drag, with full-size passenger cars. A parabolic relationship was also the conclusion here. The vehicles were equipped with spoilers to generate the forces, and the experiments showed that there was an impact if the spoiler was flush to the body or not. With the spoiler attached above the body, with a gap, the aspect ratio was related to the aspect ratio of the spoiler geometry, and not the vehicle body. An illustration of vortex cores and a vector plot of wake vortices is shown in Figure 7.

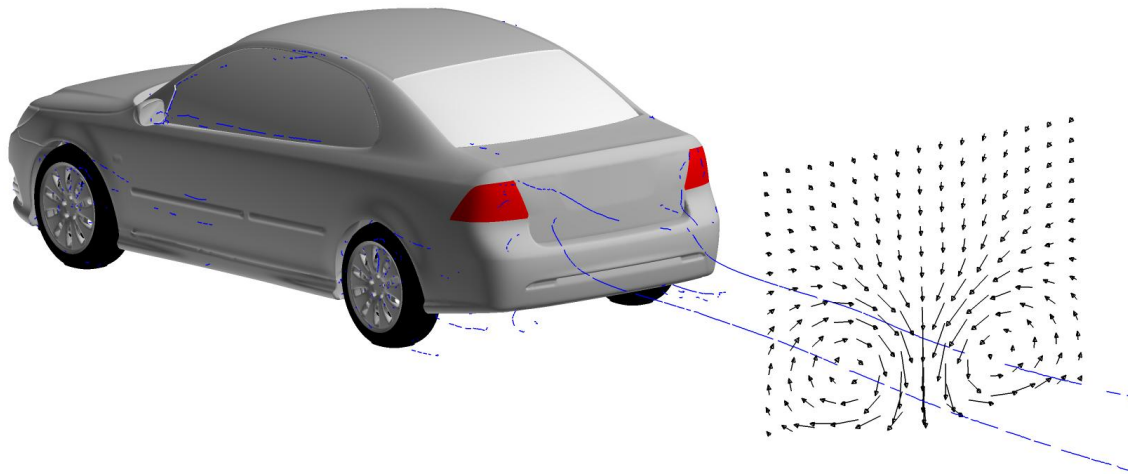


Figure 7 Illustration of wake vortices and vortex cores of a sedan car.

There is a parabolic relationship between lift and drag for a bluff body, whether there is a rough or a smooth under-body [18]. Though the under-body drag has a linear increase with increased lift for both rough and smooth under-body.

2.2. Aerodynamics of Passenger Cars

The flow around a vehicle has a stagnation point at the nose and tends to flow over and around the vehicle rather than under, due to the proximity of the ground. How much flow goes under is dependant on the ground clearance, the shape at the nose, and the rear-end shape of the body. For drag, it is most important that the shapes are rounded enough to provide attached flow around the body. Separated flow will always generate more drag than attached flow. When a rounded front-end provides attached flow, the shape of the rear-end is what determines the bluffness. It is important to have a pressure recovery over the length of the body and avoid separated flow. Tapering body dimensions, backlight angle, and under-body diffuser angle, increases the pressure along the length and leaves a base pressure as high as possible. Lowest drag is achieved with a high base pressure and a small base area.

The ultimate goals with improving the aerodynamic drag of a passenger vehicle are to reduce fuel consumption, or to increase top speed. The aerodynamic knowledge among engineers is not new, but the tools have become much better and the level of detail knowledge has increased. Also the demand for CO₂ reduction has focused attention on reducing all kinds of resistance forces including aerodynamic drag. Wind tunnels are still being used to optimize the body shape for low drag. Equipment for flow measurement and force measurements has become more advanced and the wind tunnels have been adapted to simulate the moving ground better. The technique of using wool-tufts and smoke is still employed in wind-tunnel work to visualize flow fields, but more advanced equipment is available for detailed boundary layer and wake flow analysis. The top priority for passenger cars is to minimize separated flows and have low lift forces at the rear end. Figure 8 illustrates the evolution of cars and aeroplanes with a strong influence of aerodynamics.



Figure 8 Evolution of cars and aeroplanes influenced by aerodynamics. Courtesy of Combitech AB.

In this project the primary goal was to reduce CO₂ emissions by reducing fuel consumption. A reduction of the aerodynamic drag is a fundamental source of resistance forces for the vehicle. Meaning reduced energy required for propulsion, and is independent of powertrain used. The forces a vehicle has to overcome in normal operation can be described by equation (4).

$$F_x = F_A + F_R + F_G + F_D = \gamma m \frac{dv}{dt} + f_R mg \cos \alpha + mg \sin \alpha + \frac{1}{2} \rho C_D A U_\infty^2 \quad (4)$$

F_A is the force required for the acceleration of the vehicle. This term has a substantial effect on the total driving resistance, and the acceleration is very dependent on driving behaviour and the total mass of the vehicle. The mass is m and γ is a factor for the rotating masses. The F_A is instantaneous and will have peaks of short intervals. The acceleration is specified in the driving cycles and can be positive or negative. A negative force can be re-used by brake regenerative systems in modern hybrid or electric vehicles. F_R represents the rolling resistance, and is proportional to the normal force that the tyres apply to the road, that is, the mass of the vehicle. f_R is a constant for rolling resistance but has very complex properties since it depends on tyre pressure and temperature as well as mechanical driveline losses. Also chassis properties such as wheel suspension geometry and more, that is vehicle unique. F_G is the force required to go uphill or downhill dependant on vehicle usage. And lastly the aerodynamic drag force that is dependent on air density, the form factor C_D , the frontal area of the vehicle, and the square of the vehicle speed. C_D is a form factor and a measure of the quality of aerodynamic shape with regard to drag, and the main focus in this project. The product of $C_D \times A$ is proportional to the drag force and thereby the fuel consumption, since the size of the vehicle is also considered.

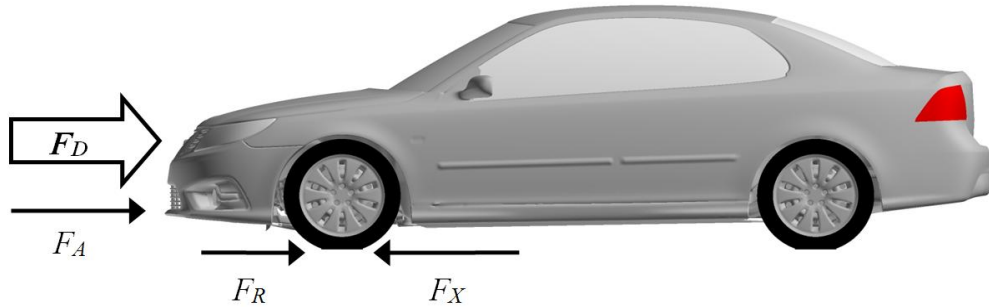


Figure 9 Illustrative picture of resistance forces.

The driving cycles for fuel consumption in the EU (NEDC) are defined using a level road with specified accelerations, velocity and driving distance. Consequently the third term (F_G) will disappear and the acceleration term will be dominant at low speed, and the velocity term (aerodynamic drag) will be dominant at high speed. For a passenger car at constant speed the rolling resistance will be dominant up to 60-80km/h and above that the aerodynamic drag will be dominant.

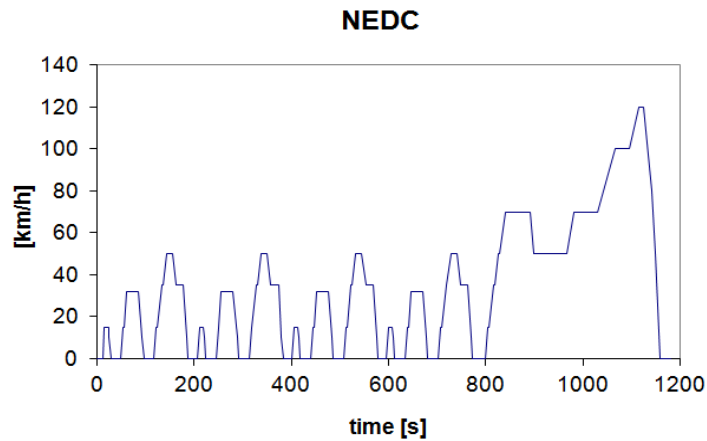


Figure 10 NEDC for certification and fuel consumption test in EU [19].

With hybrid and electrical vehicles there is the possibility to re-use the negative acceleration forces for brake re-generation. This converts the kinetic energy from the vehicle to electrical energy and can be used for propulsion. This system reduces the losses in acceleration forces and makes the aerodynamic drag even more important for fuel economy. A mild hybrid can provide 7% improved fuel economy by brake energy regeneration according to GM [20].

2.3. Aerodynamic optimization of passenger cars

When the aerodynamics are being optimized on a passenger car there are many areas to consider. A summary of the general and detail information, based on experience from Saab Automobile AB and official aerodynamic research [13] [21], is presented in this section. The focus here is mostly drag, that is, energy related, but also areas of top priority safety and comfort will be discussed. The drag-related aerodynamics can be split into four areas, even if they all affect each other. These areas are: the exterior body, the under-body, the wheels and wheel houses, and the cooling air flow. The overall vehicle preferences will give opportunity to reduce drag by optimizing:

- Total front area as small as possible. Will directly affect the drag force.
- Ride height
- Vehicle pitch angle
- Active control of cooling inlet
- Rear boot-lid profile and under-body upsweep
- Wheel to body relationship and wheel-house opening
- Low drag mirrors

The aerodynamic drag force is directly proportional to $C_D \times A$ and this makes the frontal area of the vehicle very important for fuel consumption. The ride height and pitch angle will affect the total flow field around the vehicle and also change the front area. The cooling flow through the engine-bay will also affect the global flow-field around the vehicle, since the outlet of the cooling flow normally exit to the under-body and front wheel-house. The major part of the cooling drag losses comes from the affect of the downstream flow from the cooling outlets. To actively control the cooling flow by closing them when there is no need to cool the engine, is effective. The boot-lid and rear under-body angle will control the total pressure recovery of the vehicle body and have a major impact on the bluffness and thereby the C_D . The wheels are protruding into the airflow and create a lot of turbulence due to the fact that they are rotating. To keep the outer edge flush to the body and the wheel house openings as small as possible generally reduces losses. Wheels and wheel houses are very complex areas aerodynamically with many factors interacting. Detailed study of wheel aerodynamics has been carried out by Landström [22]. The mirrors are also protruding into the air flow and should be optimized for low drag, and as small as possible in general. They must also be optimized for low wind-noise and low contamination of the side windows due to their location close to the driver and visibility requirements.



Figure 11 Picture of Saab 9-3 for illustration.

General recommendations for the main body:

1. Avoid sharp leading edge at the front. Radius $>10\text{mm}$ should be used.
2. A-pillar radius should be bigger than $r/w=0.05$, at least 60-80mm.
3. Roof leading edge should be at least 60mm.
4. Vehicle highest point should be above the driver.
5. Front end plan view sweep should be small to decrease exposure of the front wheels.
6. Plan view front corner should start with a relative small radius that increases to blend with the side.
7. Wipers parked position should be hidden below the hood line to reduce wind noise.
8. Vehicle widest point should be just in front of the driver location.

It is recommended that a sharp leading edge is avoided to prevent a separation bubble over the hood. The slope of the hood does not have a large effect and the same applies to the angle of the front windscreen. This is valid as long as the radius at the roof and A-pillar are sufficiently large. On the sides and roof there should be attached flow all the way to the rear. It is best if the shape tapers both in side view and plan view, to allow a pressure recovery as much as possible, and leave a base pressure as high as possible. Thus:

- Plan view taper angle to the rear-end should be $10-15^\circ$.
- Tyres should be as narrow as possible.
- The backlight angle should be around $12 - 15^\circ$.
- The lower sill or rocker panel should be as far out as the tyre to cover the rear wheel and to prevent gravel from the front wheel damaging the vehicle rear end.
- The trailing edge should have a sharp radius to enable a distinct separation point. This will increase stability.
- Use under-body covers to give a flat under-body.

A passenger car is a bluff body aerodynamically and the majority of the drag is pressure drag that comes from the formation of wakes and vortices [23]. BMW [24] say that approximately 40 % of aerodynamic drag comes from the basic shape and proportions of the body, 20 % from the under-body, 30 % from the wheel arches, and 10 % from the air intakes.

The exterior body of a modern passenger car is smooth, and edges and gaps are generally considered acceptable. The major wakes are related to the wheel arches and the rear-end of the car. The under-body and its interaction with the rear-end has not been as extensively investigated as the upper body. This work focuses in these areas for this reason. Unique to this work is the effect of under-body shape including under-body diffuser, on drag reduction. It is explored regarding automobile applications and in combination with different car rear-end types.

2.4. Diffuser of a passenger car

An automobile diffuser is traditionally used as a downforce generator, but it can also be effective for drag reduction for some type of bodies. The overall idea and function is that a cross-sectional area increases in the flow direction, producing a decrease in fluid velocity from inlet to outlet; with a corresponding increase in static pressure, see Figure 12. The increase in static pressure at the exit will lead to a higher base pressure that is desirable for drag reduction. The effect of the diffuser, used at an under-body, in external aerodynamics is complex. It will work with several fluid dynamic mechanisms. In a summary of diffuser theory by Cooper [25] the mechanism are described in three parts:

- Ground Interaction
- Upsweep
- Diffuser Pumping

Ground interaction - A symmetrical body in free stream has no lift force. Placing this body in proximity to the ground will result in an asymmetrical flow which will accelerate underneath the body. The flow around the body will be cambered. Static pressure at the under-body will be reduced.

Upsweep - The rear-end of the under-body will camber the flow around the body and make it act similar to an upside down wing, close to ground.

Diffuser pumping - The cross-sectional area in a diffuser increases downstream and this leads to a reduction of the air velocity. If no separation of the flow occurs, the more the cross-section increases the better pressure recovery. Most of the pressure increase will be seen as a decrease in the inlet pressure. This will increase the pressure difference from the start of the under-body to the start of the diffuser, and will increase the flow of the under-body.

The geometry, such as diffuser length and angle, will determine the pressure recovery and the relationship is well mapped for 2D diffusers [26]. In automobile applications the diffuser will be unsymmetrical and open-sided.

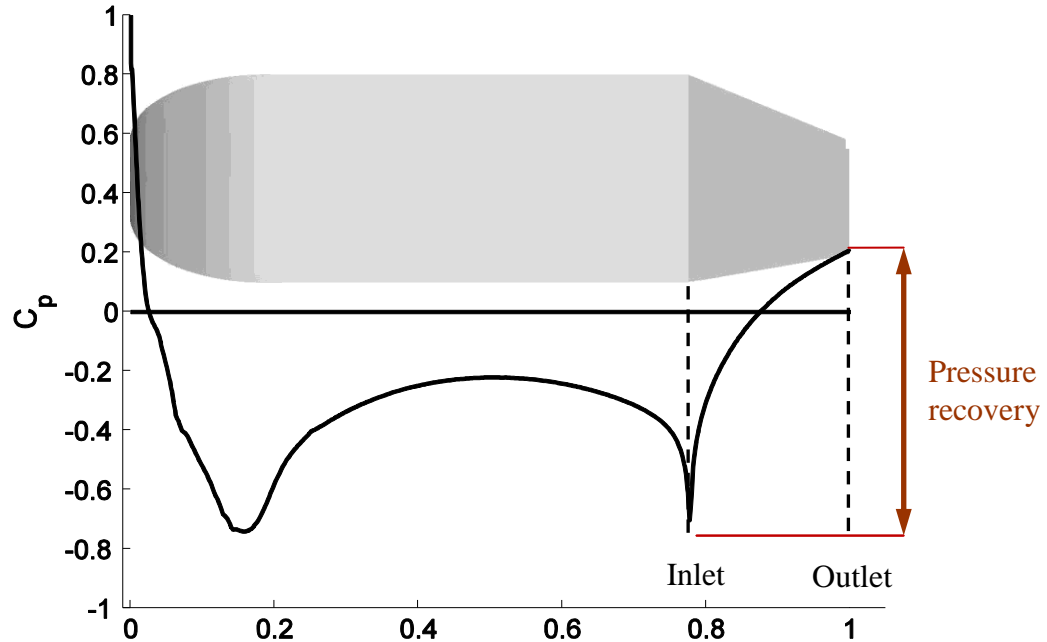


Figure 12 Schematic picture of under-body pressure with a diffuser.

The performances are not that well mapped and effect will vary with ground clearance. The function as a drag reduction device is a result of the static pressure increase of the base. The drag reduction function is depending of several parameters and is not fully known. This work includes studies in this subject applied to passenger car.

The static pressure recovery coefficient of a diffuser is defined as:

$$C_{pd} = \frac{p_2 - p_1}{\frac{1}{2} \rho U_1^2} \quad (5)$$

Where p_1 is the inlet pressure, p_2 the outlet pressure ρ is the fluid density and U_1 is the velocity at the inlet. The aspect ratio of the diffuser is h_2/h_1 and N is the diffuser length, see Figure 13.

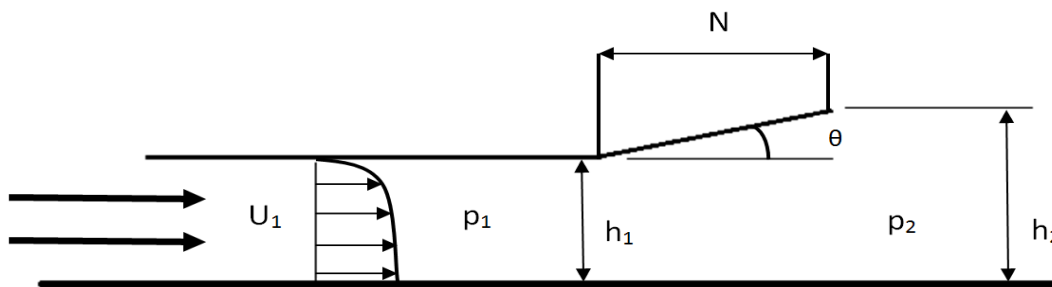


Figure 13 Schematic picture of an under-body diffuser.

2.5. Aerodynamic devices

Many different spoilers are used to control the aerodynamics of road vehicles. Exterior spoilers are located at the trunk or the rear of the roof, or at the front bumper. Reducing drag or reducing lift force are primary purposes, but they also used to improve cooling flows, comfort and function issues. Cooling flows are necessary but generate losses and additional drag for a passenger car. The total loss will come from the inlet, ducting, heat exchangers and outlet. The location and direction of outlet flows generate disturbances to the surrounding flow that will generate additional drag for the vehicle. A good design of the cooling flow outlet is desired for low cooling losses. Grille shutters temporarily block the cooling flow at low engine loads, when cooling is not needed, and actively control the flow via an actuator. The benefit is that the cooling losses are totally eliminated when it is active, and this means a 10% drag reduction in some cases. Drawbacks are that additional weight is added to the vehicle, and relative high cost. The use of active devices instead of passive devices is a balance between benefit and cost (price, mass, energy usage, packaging).

2.5.1 NACA ducts

A passive aerodynamic device for reduced drag can be to provide a desirable shape for the purpose. A NACA duct inlet is used as an inlet with high efficiency and very low additional drag for the vehicle. It must be located in an area with thin boundary layer and it should be oriented parallel to the flow direction. The idea is that air flowing towards the narrow opening flows down the ramp of the intake, and the air that approach from the outside flows over the edges of these diverging duct walls. Two counter-rotating vortices are generated when the air flows over an edge at an angle, and air will be drawn into the inlet from a diffuser effect. The edges of the duct need to be sharp to encourage the vortex formation that will draw more air into the inlet. The front edge is important and should have a radius to minimize losses and wake creation at the inlet.

The benefits are low cost and a robust design that do not need maintenance. As an air inlet it may provide a possibility to have an inlet close to the area where the air is needed and avoid long ducting. These types of inlets are used by a few car manufacturers and more widely used in race-car applications. It has been shown [27] that for automotive boundary condition, that is, low Mach numbers and a relative bluff body, the impact of the side wall radius and the inlet aspect ratio is negligible, but the lip shape, slant angle, cross-flow angle and boundary layer thickness has a great impact.



Figure 14 Illustration of submerged NACA inlet duct.

2.6. Partial drag

A moving body can be detectable over a large region by the wake flow far downstream. The distribution of pressure, velocities and vortices will be present in the wake and the losses in the flow can be measured. Conclusions can be drawn about the forces, particularly drag, by using momentum theorem and comparing energy before and after. Theories derived, for example by Onorato et al., Hackett et al. and Cogotti et.al. [28][29][30][31] divides the wake flow into three parts, containing pressure, velocity and vorticity. Eq.(6) expresses the relationship analytically:

$$C_{DA} = \int_S (1 - C_p^{tot}) dS - \int_S \left(1 - \frac{u}{U}\right)^2 dS + \int_S \left[\left(\frac{v}{U}\right)^2 + \left(\frac{w}{U}\right)^2\right] dS \quad (7)$$

Where S is the wake-plane measured, U is the free-stream velocity and u,v,w are the velocity vector components. The first term is the total pressure losses and the second is the velocity profile deflects and the third is the vorticity. This technique provides the possibility to visualize the origin of the drag, and the possibility of identifying the contribution of vortices-related drag

3. Method

Wind tunnel experiments are normally the base for aerodynamic research and development work. In this work the focus of the experiments was to measure forces and flow fields and surface pressure of four simplified bodies. Modern wind tunnels are equipped with advanced ground-simulation systems to simulate the moving ground. The Chalmers L2 scale-model wind tunnel can be operated with a static floor or with a full-width single belt moving-ground system that is described in detail in [22]. In this work moving ground was used and compared with static ground. The experiments were compared to simulated results in CFD. Results from bluff bodies were compared to results from full size vehicles.

3.1. Experimental method

The main experimental work of bluff bodies was carried out in the Chalmers L2 wind tunnel using small-scale models. Full size vehicle test were carried out in the Volvo aerodynamic wind tunnel. A brief description of the Chalmers wind tunnel follows.

3.1.1 The wind tunnel

The Chalmers L2 wind tunnel is a closed loop (vertical), closed test-section wind tunnel, with an octagonal test-section of 2.08 m^2 and dimensions of $3.00\text{m} \times 1.80\text{m} \times 1.25 \text{ m}$ (L x W x H). The contraction ratio is 5.86:1 and the speed range is 0-60 m/s. It can be used with a static floor or a full-width moving belt. The main fan has a power of 170 kW. The main fan is 2 metres in diameter with 6 wooden rotors followed by 7 stator blades which also work as flow straighteners and motor support. The main fan is air cooled and the cooling air is evacuated through channels inside the support blades. In order to compensate for this flow loss and other flow losses occurring in the test section a secondary fan unit injects air through a manifold. This air is also temperature controlled by an external heat-exchanger in order to maintain constant tunnel temperature during testing. The cooling fan has a 50 kW motor and injects fresh air into the circuit. An air-conditioning unit cools the injected air to be able to maintain a temperature control of $21 \pm 1^\circ\text{C}$.

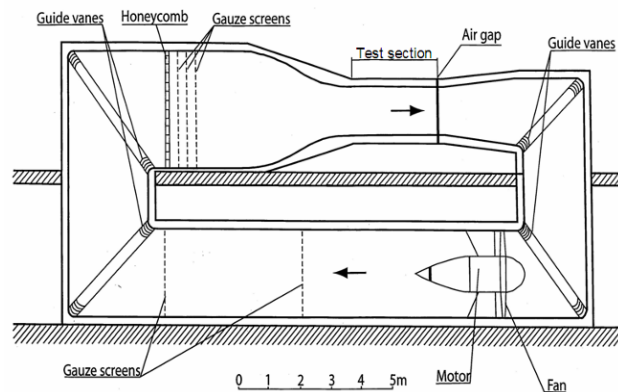


Figure 15 Chalmers L2 scale-model wind tunnel.

The test section has a divergence angle to reduce the effect of boundary layer growth along the length of the test section. The start of the test section has a boundary layer suction slot across the width of the floor, 50 mm in-front of the start of the belt. The belt is a full-width belt with a length of 1690 mm and a width of 975 mm. The rear end of the test-section has a 20 mm breather slot to equalize the pressure in the wind tunnel. The test speed in the experiments was 35 m/s unless otherwise stated. A higher test speed was possible but it was chosen as a nominal speed for the stability and repeatability of the moving ground system. A fully-automated control system using Labview is operated by the wind-tunnel computer.

3.1.2 The test models

The overall dimensions of the test models were 720 x 280 x 200 mm. The shapes were of vehicle proportions, of approximately 1:6 scale, and can be seen in Figure 16. They were generated in a free-form rapid-prototype machine at Saab Automobile using SLA (stereo-lithography). The machine was an SLA7000 from 3dsystems [32]. The models were created in three parts, with a nose section and a centre section. The rear section was comprised of four exchangeable parts that resembled four different vehicle rear-end types. The surface of the models were polished, and painted with a primer and three layers of paint, and finished with a sealing wax. The procedure was the same as normally used for prototype models and scale-model car models.

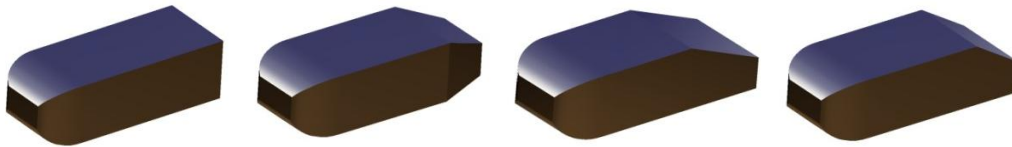


Figure 16 Simplified bluff bodies used 1. Square-back 2. Boat-tail 3. Fastback-21 4. Fastback-30.

The models were initially tested in smaller scale, 360 x 140 x 100 mm. These were made in aluminium with machine tolerances and were similarly divided into three parts with inter-changeable rear ends. The common geometric shapes and labelling is show in Table 1.

Table 1 Geometric description of the simplified test models

Case Label	Test body Model	Geometry			Size Length/Width/Height
		Backlight	Diffuser	Taper	
bt	Boattail	21°	10°	15°	3.6/1.4/1
fb21	Fastback-21	21°	0°	0°	3.6/1.4/1
fb30	Fastback-30	30°	0°	0°	3.6/1.4/1
sb	Squareback	0°	0°	0°	3.6/1.4/1

The frontal area of the larger model was 0.056m^2 and this led to a blockage of 2.7% in the test section. Frontal area of the smaller models was 0.014m^2 that led to a blockage of 0.7%. Front and side view of the models in the tunnel section is shown in Figure 17.

As stated, each model consisted of three parts: the nose of the model, rounded enough to provide attached flow along the model; the centre part, that attached to the balance; and the rear part, that consisted of four exchangeable parts. The four rear-end models shown in the right-hand picture were: fastback (30° backlight angle), boat-tail, fastback (21° backlight angle) and squareback.



Figure 17 Front and side view of the bluff-body models in Chalmers L2 Wind tunnel.

All models were prepared with 1mm diameter pressure holes along the centre-line of the models. The rear-end models had multiple holes at the backlight and at the base, to be able to measure average surface pressures. The test model was attached from above by a streamlined sting via the balance. A sketch of the boat-tailed model with main dimensions can be seen in Figure 18.

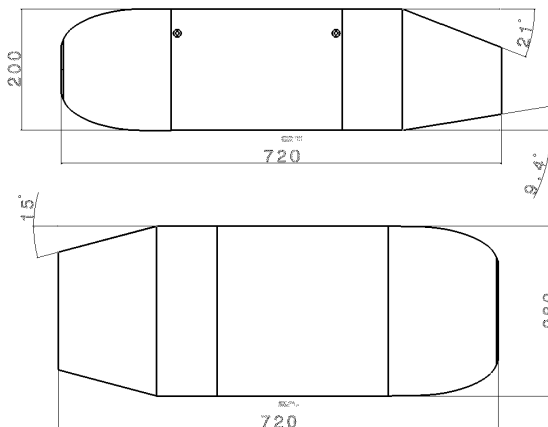


Figure 18 Sketch of boat-tail model.

3.1.3 Force measurements

The aerodynamic forces were measured with the balance mounted inside the model. A six component strain-gauge balance from RUAG, type 196-6C, was used. It was load limited to Fz 1200N Fx 350N Fy 250N, and attached to the sting in the wind tunnel. The cables were routed via a hole through the centre of the sting, up to the roof. For data acquisition there was a SCXI1600 DAQ (data acquisition) device to receive the analogue signal, amplify and digitize them. An SCXI1520 module was used for interfacing to the strain-gauge bridges simultaneously with 8-channels. The excitation voltage was 10V DC. The balance carried seven full-bridges to measure all six degree of freedoms. The measurements were carried out at 1000 Hz, and 3000 samples that gave 3 seconds per measurement point. The calibration matrix of the balance was installed with the correction method specified by RUAG in the set-up. A summary of maximum specified calibration error is listed in Table 2.

Table 2 Calibration error in all directions specified by RUAG

	F _X	F _Y	F _Z	M _X	M _Y	M _Z
Max error in ‰	6.7034	8.7341	4.0650	-2.1689	2.7040	-1.8051
Standard deviation in ‰	1.7731	2.4374	0.7355	0.4257	0.5308	0.4232

3.1.4 Pressure measurements

The pressure measurements were carried out with PSI equipment of ESP pressure scanners and DTC Initium data acquisition. The best accuracy was achieved with averaged result over 64 samples, as recommended by the manufacturer. Sampling rate was set to 100 Hz and the result was averaged over 64 samples, 4 times. This produced 4 blocks of measurement with 256 samples for each measurement,. This was repeated 5 times with 30 seconds delay which meant that a total of 20 measurements were averaged for post-processing.

The ESP pressure scanners were miniature electronic differential-pressure measurement equipment, and maintained a static error within $\pm 0.03\%$ full-scale or better. The measurements series were started with a calibration, and the scanners incorporate a two position calibration manifold actuated by momentary pulses of control pressures. The manifold automatically switched between two common reference pressures to ensure a stable reference during calibration. The scanners were placed inside the models so the tubes from the pressure taps were not more than 0.2m long. The models were prepared with pressure taps that were glued to each hole in shell of the body. The reference pressure was taken from the wind-tunnel laboratory with a tube routed through the sting. Pressurized air for calibration required tubes from an external source to be routed through the sting together with the electrical cables.

The DAQ was a DTC Initium data acquisition system for ESP scanner series from MEAS. It used an analogue-circuit design with Digital Temperature Compensation (DTC). The scanner had a static accuracy of $\pm 0.05\%$ full scale, and this included combined errors due to non-linearity, hysteresis and non-repeatability. It had a total thermal error of $\pm 0.002\%$ full-scale/ $^{\circ}\text{C}$, and a measurement resolution of $\pm 0.003\%$ full scale; according to the manufacturer. Scanner and set-up is shown in Figure 19.

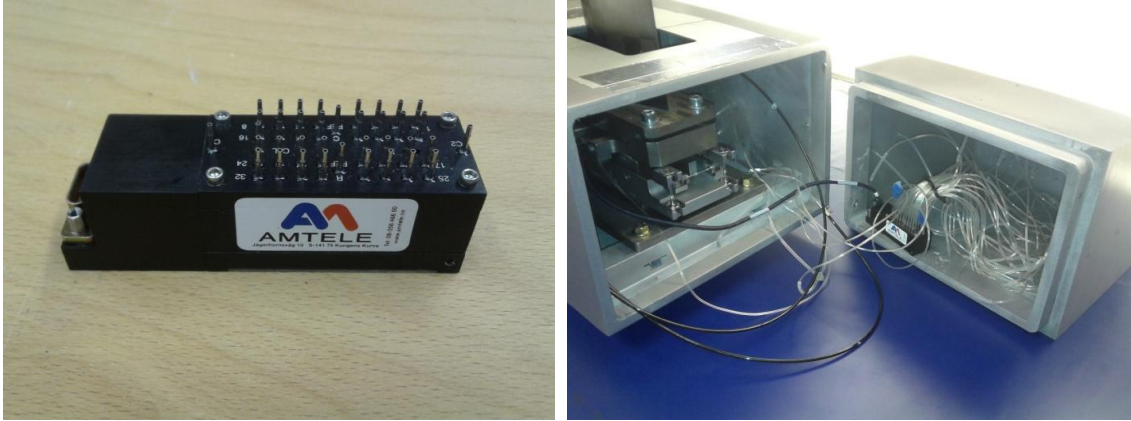


Figure 20 Pressure scanners in test model.

3.2. Numerical method

Numerical simulations were performed during this project. The simulations were carried out in RANS mode, in the commercial code FLUENT. Mainly one computational fluid dynamics (CFD) software was used and a brief description follows.

3.2.1 RANS

There are three equations governing the flow in fluid dynamics, and these are the continuity, momentum, and the energy equation. Since road vehicle aerodynamics is operating at low flow speed ($<0.3\text{Ma}$) and constant temperatures, this flow is assumed to be incompressible and isothermal. The equations can then be written in incompressible form and the energy equation can be neglected. Tensor formalism is used to describe the equations below:

Continuity equation:

$$\partial_i u_i = 0 \quad (8)$$

Momentum equation:

$$\partial_0 u_i + u_j \partial_j u_i = -\frac{1}{\rho} \partial_i p + \nu \partial_j \partial_j u_i \quad (9)$$

These two equations and the energy equation are commonly referred to as the Navier-Stokes equations. They are non-linear partial differential equations that are not analytically solvable except for some special cases at low Reynolds numbers. The simplest engineering approach is the Reynolds decomposition where the instantaneous velocity is split into a mean part and a fluctuating part. This decomposition used for velocity and pressure will look like the following:

$$p_i(x_i, t) = P_i(x_i) + p'_i(x_i, t) \quad (10)$$

Here the capital letters refer to the mean quantities and the lower case denoted with a prime refers to turbulent fluctuations. The mean velocity is defined as the time average for a period T that is long enough to get an accurate value.

$$U_i(x_i) = \frac{1}{T} \int_0^T u_i(x_i, t) dt \quad (11)$$

The decomposed terms are inserted into the governing equations and time averaged. The resulting equations are known as Reynolds Averaged Navier-Stokes equations and normally referred to as RANS equations.

$$\overline{\partial_i u_j} = \partial_i \bar{u}_j = \partial_i U_j = 0 \quad (12)$$

$$\rho \partial_j (U_j U_i) + \rho \partial_j (\overline{u'_j u'_i}) = -\partial_i P + \mu \partial_j \partial_j U_i \quad (13)$$

This momentum equation governs the time-averaged properties of the flow. It contains a new effect, $\rho(\overline{u'_j u'_i})$, called the Reynolds stresses. New unknowns have been generated and the number of equations is not enough to solve the problem. This is called the closure problem and it is the reason for modelling the Reynolds stresses with

turbulence models. There are several different methods to model the Reynolds stresses. A common method is the Eddy Viscosity model: that links the velocity gradients via the turbulent viscosity. The model is simple, stable and works well for many engineering purposes. The k- ϵ model is an eddy-viscosity model where the modelled transport equation for the turbulent kinetic energy, k, and dissipation, ϵ , are solved. In the derivation of the k- ϵ model the assumption is that the flow is fully turbulent, and the effect of molecular viscosity is negligible. The standard k- ϵ model is therefore valid only for fully turbulent flows. The realizable k- ϵ contains a new formulation for turbulent viscosity involving C_{μ} and a new transport equation for the dissipation rate. An immediate benefit of the realizable model is that it more accurately predicts the spreading rate of both planar and round jets. It provides better performance for flow involving rotation, boundary layers under strong adverse pressure gradients, separation and recirculation [33]. The k- ϵ realizable has been used for simulations performed in this work.

3.2.2 CFD approach

The simulations were performed to the simplified models and to full scale passenger vehicle models. The surfaces and the surface meshes were prepared in the commercial code ANSA for all cases. The volume mesh was generated in Tgrid and the simulations were carried out in Fluent. Post processing was done in FLUENT, FieldView and Matlab. The same software of different versions was used during the project.

3.2.3 Boundary conditions

The boundary conditions differed depending on whether simplified models or full-size cars were simulated. The bluff bodies were compared with wind tunnel measurements carried out in the Chalmers wind tunnel L2, and therefore the geometry of the wind tunnel domain was used as Digital Wind Tunnel. For the full-size cars a more conventional oversized wind tunnel domain was used.

The boundary condition of the wind tunnel domain for bluff bodies was a moving ground, and solid walls and roof. The inlet was a velocity inlet set to 5.75 m/s that made the air speed at the Prandtl tube 35 m/s. The breather slot of the wind tunnel was simulated as a part of the domain, and the wind tunnel laboratory was used as a volume to provide the reference pressure. The boundary conditions of the volume in the wind tunnel laboratory were pressure outlet defined as 0 Pa, except for the floor that was defined as a wall. The belt was assigned a translational speed of the same magnitude as the free stream air: 35m/s. The wind tunnel outlet was assigned with a pressure outlet specified at 550 Pa. The solver used was Fluent V14. Simulations were carried out in RANS (Reynolds Averaged Navier Stokes) mode, pressure based with the k-epsilon realizable turbulence model. Non-equilibrium wall functions and a simple pressure-velocity coupling were used. First 500 iterations of first order upwind differential scheme was used, then 2500 iterations of second order upwind. 3000 iterations were performed for each case and it was considered converged when the variation was ± 1 drag count and the residuals where stable below 10^{-3} . The presented coefficients are an average from the last 200 iterations.

The test model and sting in the wind tunnel domain is shown in Figure 21. The breather slot is visible as a gap in the wind tunnel behind the test body. Location of the

Prandtl tube for air speed and reference pressure in the wind tunnel was used for reference speed to the coefficients.

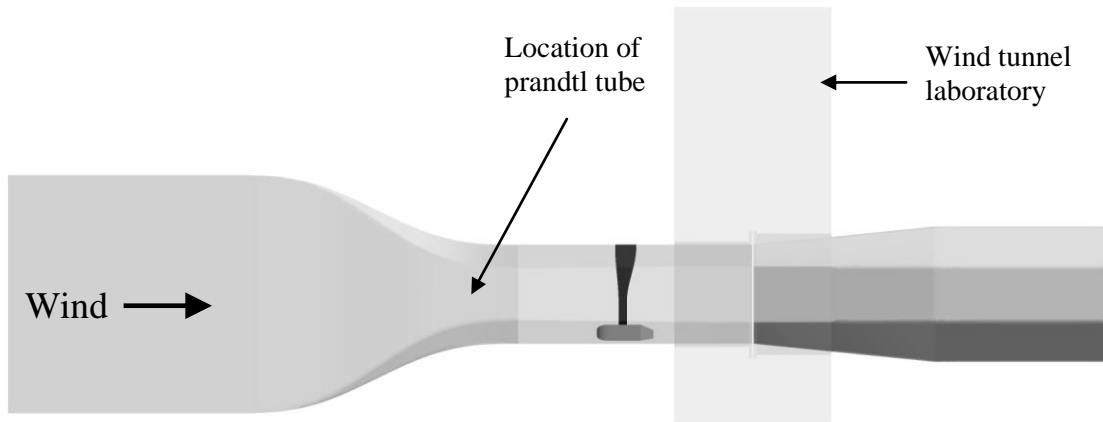


Figure 21. Simulation domain and test model

3.2.4 Simplified models

The surfaces and the surface mesh were prepared in the commercial code ANSA. The resolution of the surface mesh was approximately 2mm to give the right geometry for the prism layer. The volume mesh was generated in Tgrid 13.0, with a prism layer of 15 layers and an aspect ratio of 5 from the surface mesh. The size was selected to maintain a y^+ of more than 30, as recommended by Fluent [33]. The prism layer was applied to the models and the sting. The walls, roof and floor of the wind tunnel also had a prism layer but only 5 layer were used here. The size of the surface triangles was from 5 mm to 100 mm, with the smaller used at the floor close to the model, and the larger at the wind tunnel walls and roof. The volume mesh was a hexcore mesh with refinement zones for the under-body and wake region. The simulation domain in the outlet diffuser area of the wind tunnel domain was elongated by the length of 1 tunnel diameter to stabilize the flow at the outlet. The total mesh size was 55 million cells; the mesh close to the model can be seen in Figure 22.

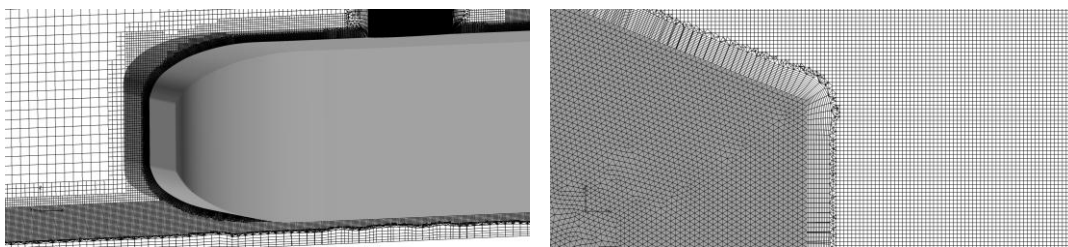


Figure 22 Example of surface mesh and volume mesh of the simplified body.

3.2.5 Vehicle models

For the full-sized vehicle models an oversized and rectangular wind tunnel domain was used. The simulation domain had a length of approximately 13 vehicle lengths, a width of 11 vehicle widths and a height of 8 car heights: to remove the need for corrections for blockage. Boundary condition of the wind tunnel was a moving ground

where the complete ground was moving. Walls and roof were set to symmetry. Final mesh size was approximately 65-70 million cells dominated by hexahedrals.

The mesh was prepared so that the only changes between the different set-ups were the under-body geometry with a variation of the diffuser angle. The resolution of the surface mesh was between 4 and 10mm to resolve suitable details and have required quality for the prism layer. The volume mesh was generated in Tgrid 14.0 with a prism layer of either 5 or 15 layers and an aspect ratio of 5 from the surface mesh, to maintain a y^+ of more than 30, as recommended by Fluent [33]. The prism layer was applied to the exterior body and the smooth under-body covers. The volume mesh was a hexcore mesh with refinement zones for the under-body, wheels and wake region. An overview of the volume mesh can be seen in Figure 23. The cooling module, condenser, charge-air cooler, radiator and fan shroud were simplified to one volume, and the mass flow was tuned by adjusting openings to the correct flow through the cooling pack and the engine bay. The simulations were carried out at 38.89 m/s to represent the wind tunnel test speed 140 km/h.

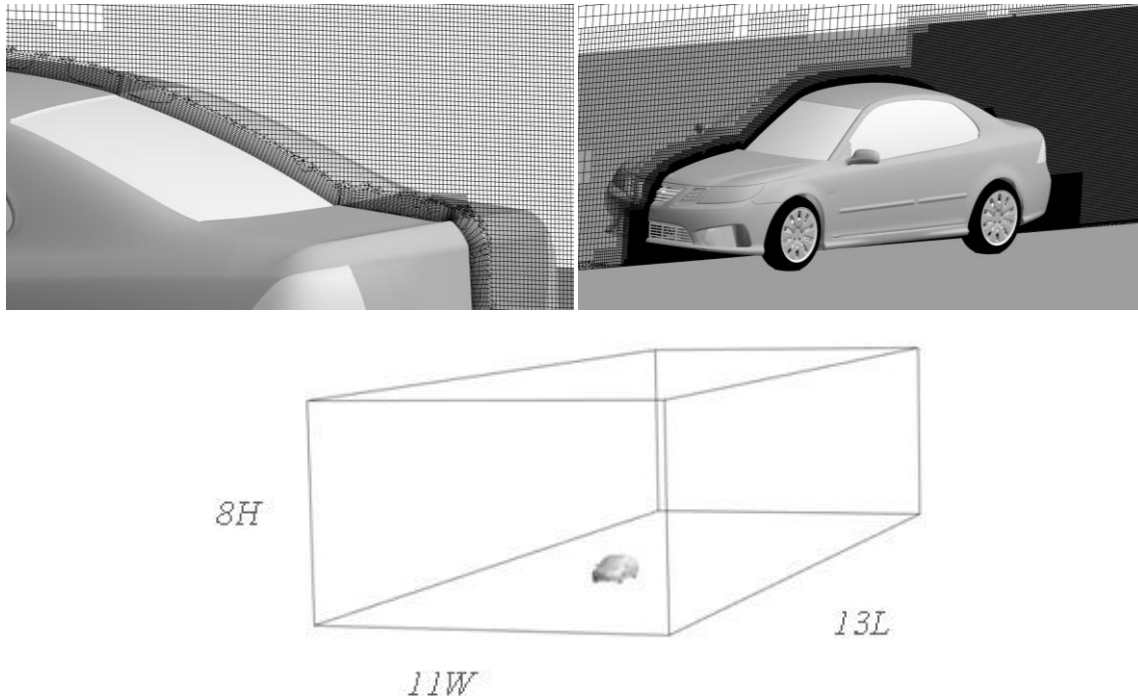


Figure 23 Mesh close to the car and digital wind tunnel domain.

The solver used was FLUENT and the simulations were specified as pressure based with the k-epsilon realizable turbulence model. Non-equilibrium wall functions and a simple pressure-velocity coupling were used. 3000 iterations were performed for each case and it was considered converged when the variation was ± 1 drag count and the residuals were stable below 10^{-3} . The presented coefficients are an average from the last 200 iterations and the reference area was the same standard values as used in the tests. The wheel rotation was simulated with MRF (multiple reference frame) and the wheel dimension and camber angles were the same as the test car. Wheel geometry, such as radial and axial expansion, will change with wheel rotation speed. This was not corrected for in this study and instead the original shape supplied from the supplier was used. The

tread of the tyre was simplified as flat surfaces since it was more important to have the same wheel geometry for all simulations.

3.3. Comparing CFD and measurements

Aerodynamic properties of passenger vehicles are determined from mainly three methods: Wind tunnel measurements, CFD simulations, and road tests. For detailed analysis, data from the first two are mainly used. There are different benefits with the selected methods, and the best is a combination of all of them. There is always a question about the pros and cons between wind tunnel and CFD in vehicle development. Both offer a variety of possibilities and opportunities, and a summary is therefore proposed in Table 3. Additionally, what is not included here is cost for operation and investment. This was intentionally left out because it depends on what level of detail and performance is being compared. Assuming equal total cost and comparing general properties the following is valid:

The main differences are that, in CFD the flow physics are modelled and include errors due to software, mesh, user set-up and numerical accuracy. In a wind tunnel the flow is measured but has errors due to geometry, boundary conditions, and wind tunnel properties. Measuring flow properties is dependent on test equipment, for both accuracy and output speed, but generally only done for selected locations and properties. A CFD simulation on the other hand, has unlimited flow information about the specific case, once a simulation is done. A CFD simulation works with exact geometry from CAD and it is relatively easy to model boundary conditions, such as moving ground and open-road environment, including rotating wheels. A wind tunnel measurement requires more effort and equipment to model moving ground and rotating wheels, even though that is now standard practice. There are also problems with accurate open-road conditions, to reduce wind tunnel effects like blockage and buoyancy effects. On the other hand a wind tunnel has the correct physics of the flow, and naturally handles fluid structure interaction, such as deformation of body part or wheel deformation, due to flow or kinetics. It tends to be time consuming and expensive to build a test model, but on the other hand relatively quick to measure forces and make several design iterations, once the test objects are available. At the time of writing, there is still higher credibility from wind tunnel measurements and it is therefore often used for validation, especially for drag and lift. The location of the wind tunnel can make it more of a problem to transport test models and staff, while simulation tools are more portable and thereby also the staff. All in all, it could be concluded that simulations are better in the early phases of a vehicle development program, and the wind tunnel is more useful in later phases. Both complement each other and are very much needed together.

Table 3 Comparison of Wind tunnel test and CFD simulation

CFD	Wind tunnel
Physics are modelled	Physics are measured
Unlimited flow information	Selected information about airflow
Quick to build first model (relatively)	Quick to make design changes
Exact geometry (CAD design)	Mockup and clay designs
Any operating condition (incl. b.c.)	Limited to laboratory capability
Portable tools and staff	Difficult to transport equipment
Analyze concepts	Analyze details
Development for aero	Validation, high credibility for aero
More usable in early phase	More usable in later phase

4. Results

This chapter is a summary of the most relevant results in the appended papers of this thesis, with some complementary results. First results regarding bluff bodies from paper III are discussed including measurements and simulations. Then the most relevant result of the full-size vehicle and their relevance to bluff body result. Full-size wind tunnel test results are limited in this work so the comparison to CFD results of full-size vehicles is only briefly discussed. Attention is given to the under-body, rear end and the wake of all the bodies.

Different rear-end types of vehicles have different flow characteristics and vortex formations. This work started with the measurement and simulation of the bluff bodies to identify the local flow-field and aerodynamic characteristics. The improvements were tested on the body and finally tried on full-size vehicle simulations. With this information there were several combinations to test in simulations and evaluated for drag reduction. All simulations and wind tunnel tests were carried out with moving ground unless otherwise stated.

4.1. Characteristics of bluff body rear-end models

If a symmetrical body is brought close to the ground, the drag of the body will increase. The reason for this is that the flow loses its symmetry around the body as the gap between the ground and body blocks the flow. The stagnation point in the front is moved down and separation occurs earlier on the upper side. The flow around the body is cambered and the effective thickness h/l of the body increases [34]. The corresponding length to height ratio of a passenger car is approximately $l/h=3$, which is within a range where pressure drag dominates. Drag and lift depend not only on ground clearance but also on the angle of attack and yaw angle. For drag there is normally one minimum for both angle of attack and yaw. Lift is reduced with increased ground proximity but the gradient for different angles of attack has a non-linear relationship to the shape of the body.

The four rear-end models were measured with regard to drag and lift in several operating conditions and different boundary conditions. Examples from these measurements are discussed in this section. The bodies were tested in two different scales with static ground. The small scale had a length of 360 mm and was tested at a Reynolds number of 1.32 million. The larger models were double the size and were tested at a Reynolds number of 2 million based on model length. The difference between the measurements was that the larger models were attached from the top and had the balance placed inside the test body, and the smaller models were attached from underneath and had the balance located under the floor. They were measured with the same type of balance. Results for drag and lift are presented in Figure 24. The Reynolds effects affected the results and the result spreads for the models. It was therefore difficult to extract one trend from one single effect. The most obvious difference was the fastback-30 with higher drag and lift for the larger model. The smaller models generated separated flow over the backlight and the larger models had attached flow due to higher Reynolds number. This again highlights the importance of Reynolds number for scale-model testing, and the result was extreme in this case. The 30° backlight angle is known to be a critical angle [35] and produced different result in this Reynolds range. Another influence

was the boundary layer of the wind tunnel floor. The same geometric ratio of a ground clearance 0.2 of model height, as used in this example, had a larger part of the under-body flow affected by the boundary layer for the small models. When the ground clearance of the large model was reduced, the drag reduced to some extent, but not close to the difference of boundary layer separation from the backlight. A reduced Reynolds number for the larger models, by reduced wind tunnel speed, did not generate separated flow at the backlight so the conclusion was that it was a combination of the two. The boat-tail and fastback-21 had reduced drag and lift with increased Reynolds number, as expected, and the square back only had very little scale-effects. The difference in lift forces of the boat-tail model was due the boundary layer of the wind tunnel and the diffuser effect.

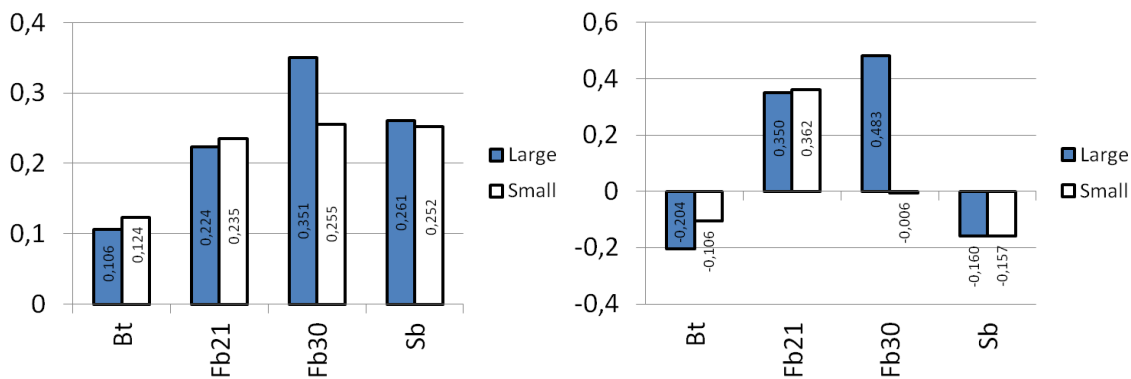


**Figure 24 Measurement result of small and large bluff bodies in CWT with static ground
Left: Drag. Right: Lift.**

The large models were measured with static and moving ground and the drag was always higher for static ground. The difference was not the same for the different rear-ends, and clearly the wake flow had a significant impact. The largest difference was found for the fastback-30 model due to the very cambered flow, and the increased under-body flow, due to moving ground, straightened the wake. The moving ground lowered the lift for all rear-ends, but it had the smallest effect to the square-back since the wake flow was relatively symmetrical for the base model.

The boat-tail had the largest lift effect from the ground simulation. This being related to the diffuser on the under-body and the boundary layer of the floor. With a static ground there is a boundary layer at the floor that is not there with the ideal moving-ground. The boundary layer will be compressed under the body but it will increase again after the body. The diffuser will increase the static pressure over its length and direct the flow upward. This will cause the boundary layer to grow even more and eventually it will merge with the wake flow. This has a large impact from the diffuser upswEEP, and the flow will have a big camber difference around the body that will generate a larger difference in lift. Figure 25 shows the C_p of total pressure in the symmetry plane from a CFD simulation with optimum boundary conditions: that is, an oversized wind tunnel domain with no blockage, and a moving ground over the complete domain length, that generated no boundary layer.

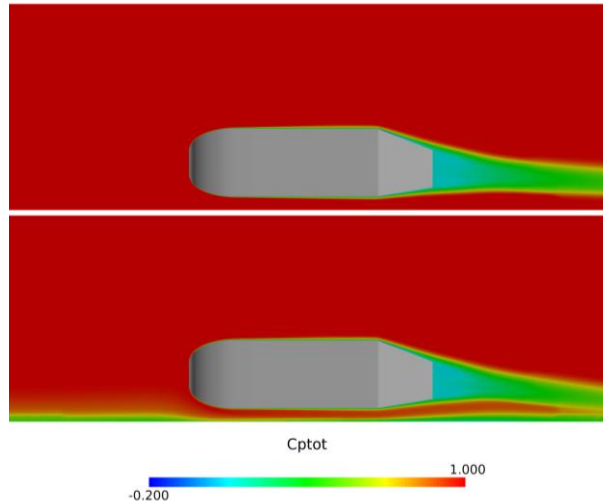


Figure 25 C_p of total pressure in symmetry plane with and without moving ground. Upper: With moving ground. Lower: Without moving ground

The results in Figure 26 are averaged from three different measurements where the bodies were dismantled and re-installed in-between. The average standard deviation of the result was C_D 0.001 and C_L 0.009, for the static ground. For the moving ground the standard deviation was 0.002 for C_D and 0.012 for C_L . The deviations were higher for the moving ground situation, but the effects for lift is more obvious. The errors were measurement uncertainties from electrical and mechanical systems and included the geometrical set-up. The importance of the pitch-angle accuracy was greater for lift compared to drag. There errors from the coefficients were larger due to the geometric ratio between frontal area and plan view area. Lift forces act relative to the plan view areas, and pressure drag relative to the front view area. The plan view area was 3.6 times larger than the front view area and all the coefficients are normalized with the same frontal area.

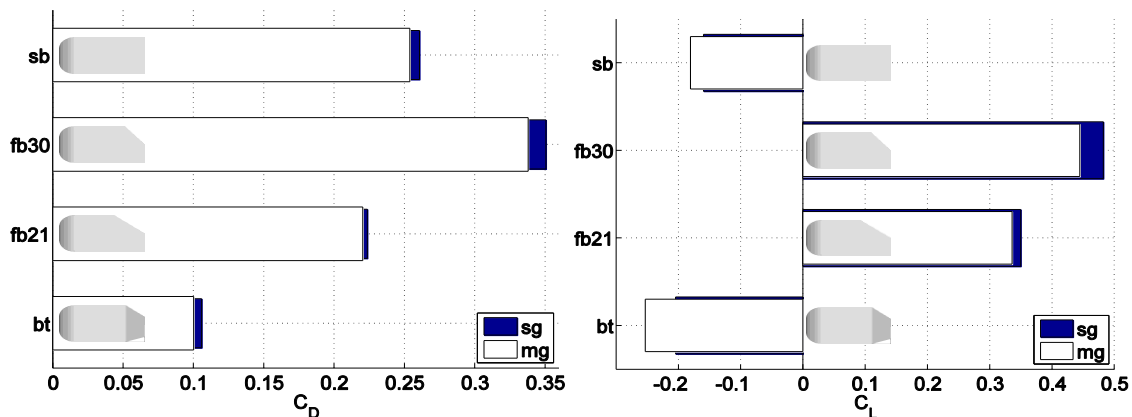


Figure 26 Drag and lift of the four bodies with static and moving ground.

The bluff body measurements were compared to simulated results in CFD. Traditionally the prediction of drag in RANS simulations, relative to measured results, is acceptable for bluff bodies and passenger vehicles. Results within 5% are good for absolute result. But prediction of lift forces are more difficult and have a larger spread in

general. Wind tunnel result is not compensated for wind tunnel effects here. The wind tunnel effects has an impact, and for that reason the wind tunnel domain is modeled in CFD. Simulations of the same models are also carried out with an oversized wind tunnel domain for comparison. Simplified bluff bodies as used here has minimum deviation from test models and will give no input to a comparison. In simulations the numerical effects are critical since the physics is modeled and detail resolution is individual and user defined. RANS simulation with $k-\epsilon$ turbulence models and wall functions has a tendency to overpredict attached flow [14] in critical angles. One effect of this will be an over-predicted lift force, especially if the critical angle is on the upper side of the body. All simulations over-predicted lift forces and the results are shown in Figure 27. Smallest deviation was found for the squareback due to no critical angles. The wind tunnel effects had a significant impact and the result with Chalmers Wind Tunnel (CWT) geometry as digital wind tunnel domain was closer to measured result. s(CWT) was simulation with the digital wind tunnel domain as geometry of Chalmers Wind Tunnel. s(sq) was simulation in over sized rectangular digital wind tunnel. Results from the fastback-30 has a big deviation and was considered unreliable. In simulations the residuals were high and convergence criteria is not fulfilled. The spread within the last 200 iterations was more than 20 drag counts and for lift even more. Acceptable simulation result with 30 ° backlight angle can not be reach with this simulation method.

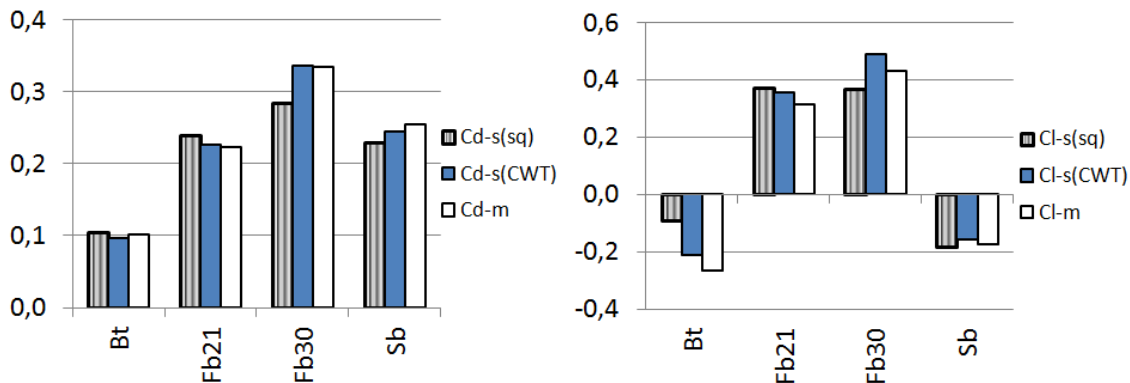


Figure 27 Measurement and simulation result of the large bluff bodies with moving ground. Left: Drag. Right: Lift.

The drag force arises from the friction in the fluid and is seen as pressure and friction forces. The division can be written as; $C_D = C_{Df} + C_{Dp}$ where C_{Df} is the friction-induced drag and C_{Dp} is the pressure-induced drag. The viscosity affects the body as friction, and generates tangential forces to the body, in the flow direction. The pressure forces also exist due to viscosity, but relate to other phenomena and will be generated by different velocity in the fluid and flow separation. The forces act normal to the surfaces in any direction. Figure 28 shows the division of friction and pressure forces for the four models in the simulations. The friction forces were approximately $C_D 0.05$ regardless of rear-end shape of the model, but the pressure forces increased with size of wake and vortices.

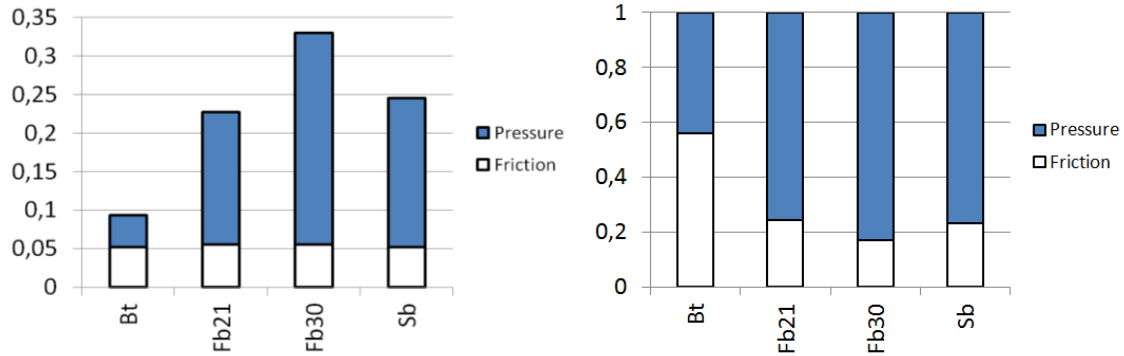


Figure 28 Pressure and friction coefficients of the four models from CFD with CWT as digital wind tunnel.
Left: Absolute result. Right: Relative result.

A square-back model as reference was not the geometry of highest drag but it represented the boxiest shape. To reduce the pressure drag it is important to enable a pressure recovery both in side view and plan view. A demonstration using bluff bodies is plotted in Figure 29. A backlight angle of 21° will reduce drag 10%. Additional plan view angles such as taper angles of 15° enables pressure recovery of the sides and reduces drag 30% more. If a 10 degree diffuser is added, the drag is reduced another 20%, in total giving 40% of the square-back. A small change in the geometry, by adding a diffuser, will have a big effect on the drag. It makes the wake more symmetrical at the same time as it creates a pressure recovery on the under-body. Straightening the wake reduces vortex induced drag by reducing longitudinal vortices. The effect of the diffuser will not be the same for another ground clearance or a smaller backlight angle due to a different wake asymmetry.

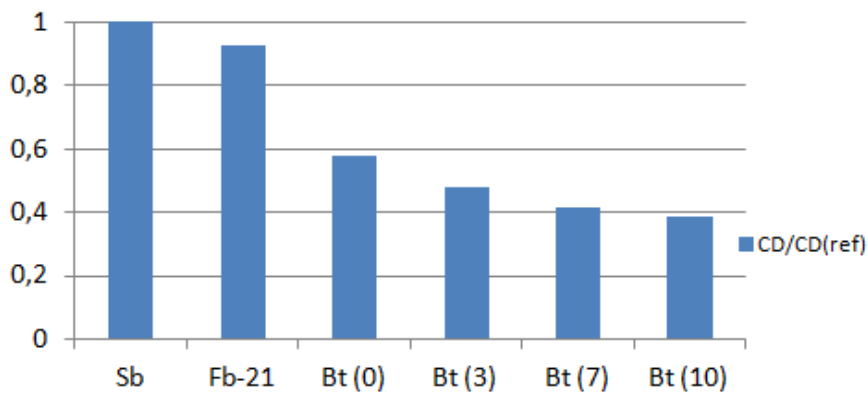


Figure 29 C_D relative to the square back model from CFD simulation with moving ground.

In paper III the simplified models were tested for wind tunnel effects, geometric impacts and ground proximities. The ground proximity changes the flow field around a body and the behaviour for drag and lift is different for different rear ends. Typically being caused by the difference in how the flow cambers around the body. From Figure 30 it is shown that the fastback models had reduced drag with increased ground proximity. The ground accelerates the air under the body and reduces the asymmetry of the wake.

The square-back and the boat-tail had increased drag with increase ground proximity because the flow asymmetry. The lowest drag is achieved when the wake is most balanced behind the body. The relationship for lift was simpler, with reduced lift for increased ground proximity, as presented in Figure 31. The exception being for very small ground clearances where viscous effects at the under-body becomes significant. The lift decreased almost linearly with more cambered flow around the body. The boat-tail model had a stronger gradient of lift reduction with increased ground proximity compared to the other models, due to the diffuser shaped rear under-body. The diffuser pumping effect was increasing the under-body flow and reducing the under-body pressure with increased ground proximity.

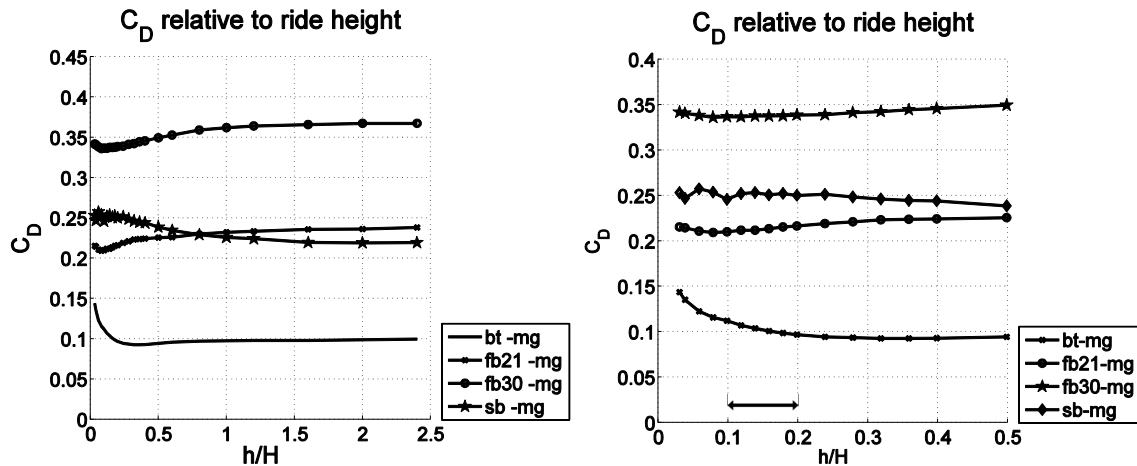


Figure 30 Drag as a function of ground clearance for the four models. Ground clearance h/H 0.2 is high-lighted because it represents the range of passenger vehicles. Measured with moving ground.

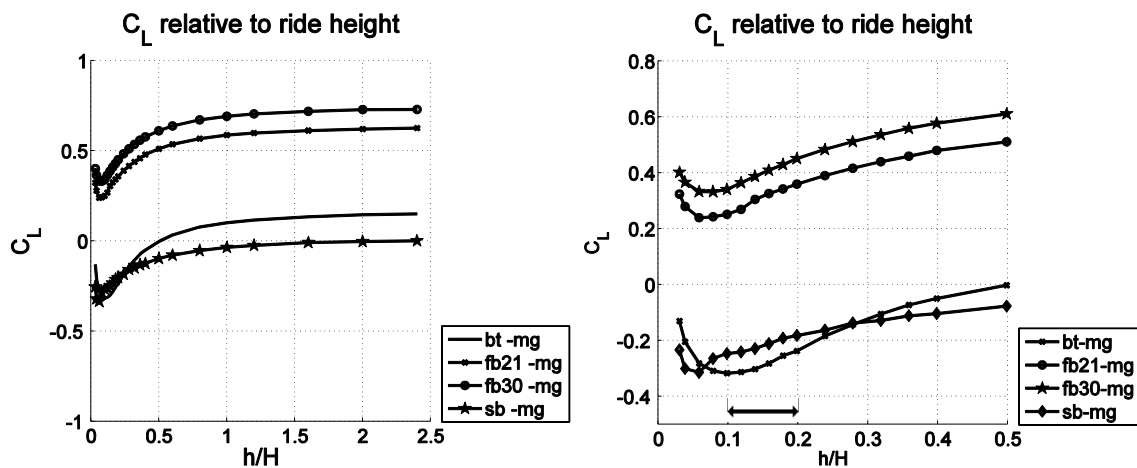


Figure 31 Lift as a function of ground clearance for the four models. Ground clearance h/H 0.2 is high-lighted because it represents the range of passenger vehicles. Measured with moving ground.

Pitch and yaw angles have a major effect on the aerodynamic forces. The bluff bodies were tested at $\pm 2^\circ$ pitch angle, to measure the effect of pitch angle to drag, lift and ground clearance. This range was chosen to represent the variation of passenger vehicles

due to type and loads. The rotation point was chosen to be at the nose of the model, and the reference ground clearance was $h/H=0.2$. Positive pitch angle was defined as nose-up attitude. In Figure 32 the effect of pitch angle to each model type is shown. All the bodies had increased lift with increased nose-up, pitch angle. This follows wing theory in free stream, meaning increased lift with increased angle of attack. Drag was systematically increased with increased angle of attack (nose-up). This meant that drag always drops with reduced angle of attack, within this span, regardless of rear-end shape. From aviation theory this would not necessarily be the case for the square-back, but the proximity of the ground changes the flow field around the body and changes the flow behaviour. The main body of a conventional passenger car always benefits from a nose-down pitch but the total vehicle effects are also dependent on the impact of the wheels and cooling flows.

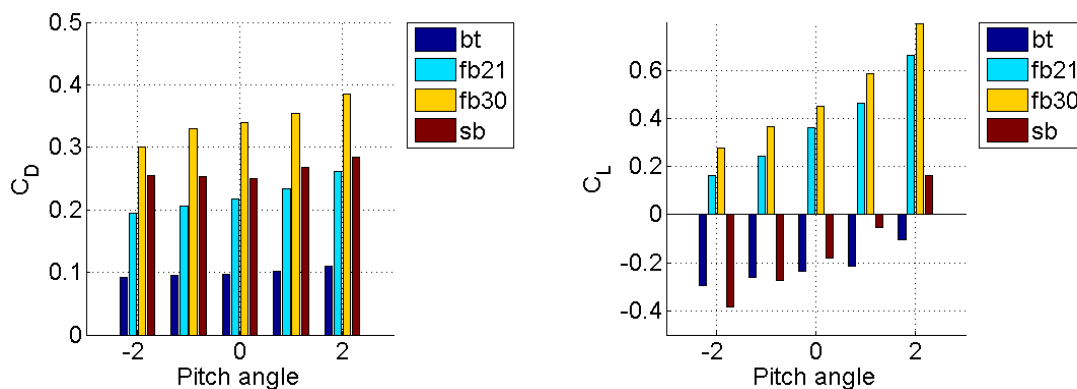


Figure 32 Drag and lift of the four models depending on pitch angle. Measurement in Chalmers wind tunnel L2 with moving ground.

Decreased pitch angle of up to 2° nose down decreased the drag force for all models. An increased nose-up pitch had a linear increase of the lift force. The different rear end types reacted differently to ground proximity for 2° nose up attitude. The drag was reduced for the square back around nominal ground clearance but had an un-linear trend. The fastback-21 reduced drag until $h/H=0.2$ and from there unchanged with increased ground proximity. The drag of the boat-tail is lower than the others and it increases with increased ground proximity around nominal ride height. The ground effects become very un-linear because the rear end will come very close to ground and block the under-body flow. For the 2° nose-down attitude the fastback models had an almost constant drag, for increased ground proximity, and a strong increase at small ride heights. The square-back and the boat-tail had a drag increase around nominal ride height, with increased ground proximity. The lift had a simpler relationship for ground proximity for various pitch angles. All models had increased ground proximity effects and reduced lift forces with more nose-down pitch. The boat-tail followed a different behaviour with smaller lift effects due to changed pitch angle. A smaller base wake and reduced impact of the diffuser effects for different body pitch being the reason. The diffuser pumping effect was reduced significantly due to the reduced area ratio of the diffuser, while at the same time the under-body of all the other models had a diffuser effect.

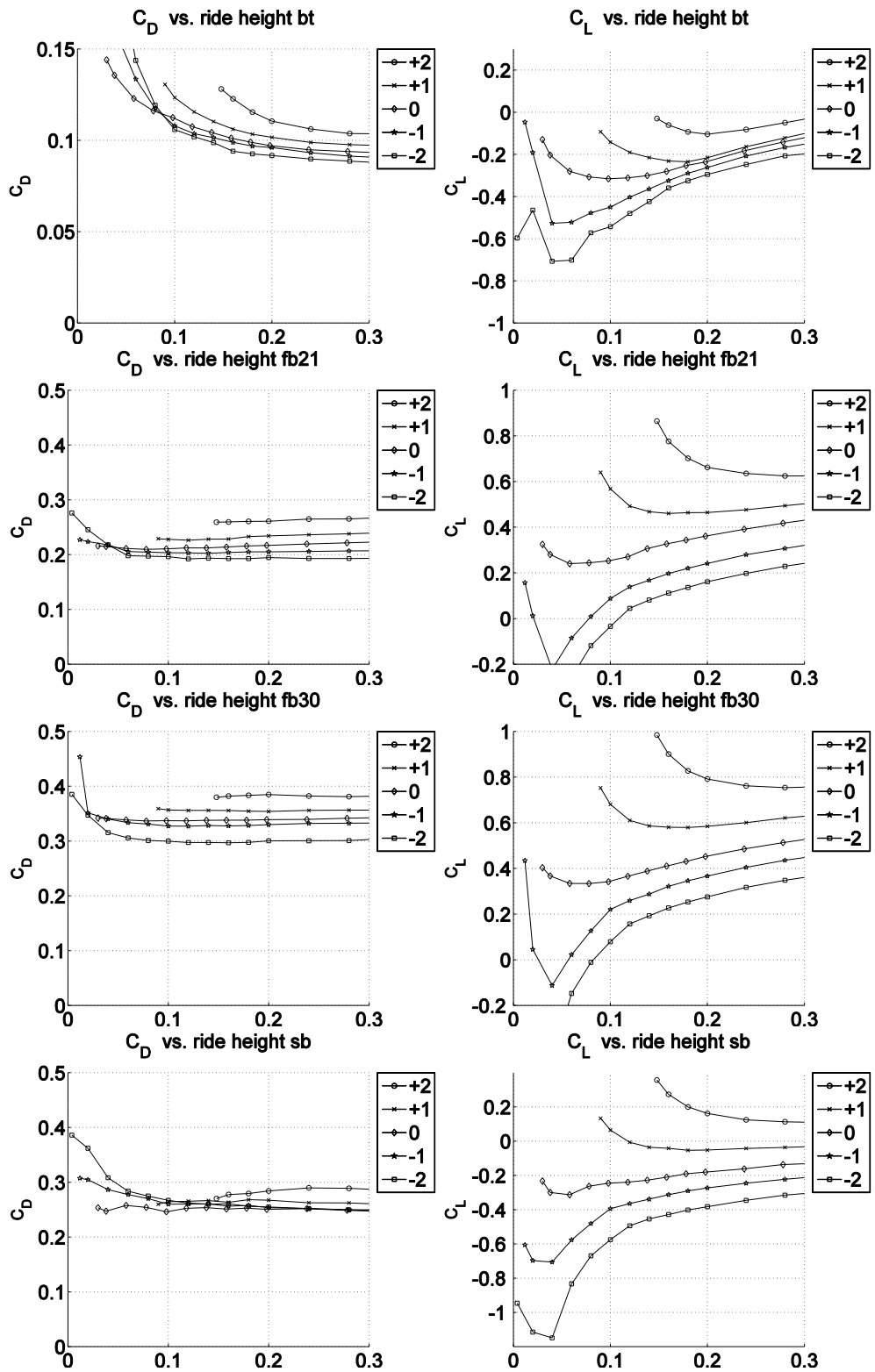


Figure 33 The effect of ground proximity for various pitch angle of the four bodies.
 From top to bottom: Boat-tail, Fastback21, Fastback30 and Square back.
 Left column: Drag. Right Column: Lift.

In paper III the general effect of small yaw angles was discussed from a bluff body point of view. The effect of yaw, depending on rear-end type, was studied for the same models. The range of yaw angles was chosen because it represented the average wind during day-time in the USA. The average wind was 2.05m/s at 2.1m above the road surface, [13] and this is considered side-wind. At normal driving at 30m/s, this resulted in a side-wind angle of 4°. The drag was increased more with larger base wake, such as the square-back, compared to the others. The increase for the square-back was up to 12 % and for the others less than 5 %. The opposite result was found for lift forces, where the square-back had significantly less lift effects than the others. This had more to do with the lack of backlight angle and diffuser angle of the square-back, that led to a smaller variation in up-sweep or down-sweep due to yaw. The results are shown in Figure 34.

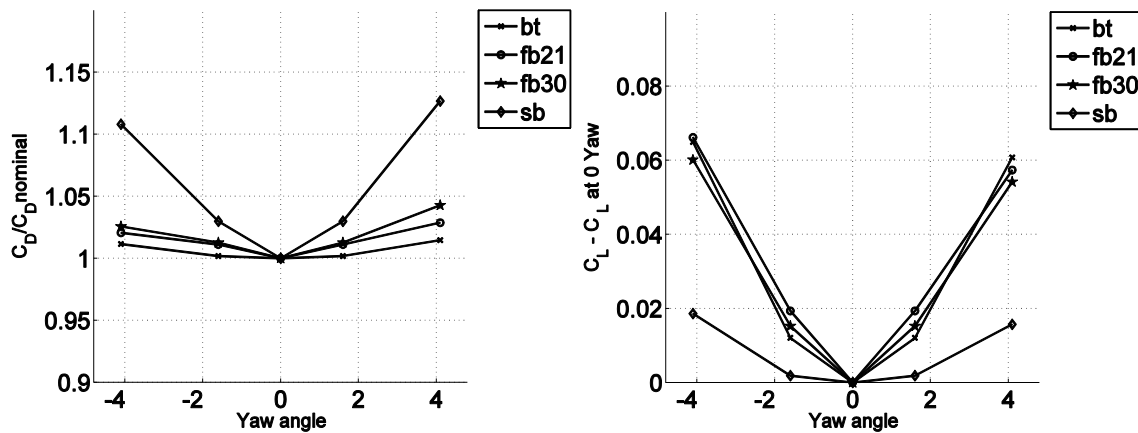


Figure 34 The effect of $\pm 4.1^\circ$ yaw angle to the rear end types.
 Left: Drag. Right: Lift.

The surface pressure of the under-body was reduced with increased ground proximity, and the under-body pressure of the boat-tail model was significantly reduced by the diffuser. Also, the effect of increased ground proximity was more obvious at the rear-end of the boat-tail which meant a reduced rear axle lift of a car. The upper-body pressure was also reduced with increased ground proximity but the magnitude was smaller. The reduced lift from reduced ground clearance was an effect of lower under-body pressure rather than any change in the flow of the upper body. The upper body was also affected since the stagnation point at the front was moved down with reduced ground clearance. The base pressure was the mean pressure of all probes at the base and the same mean pressure was used for the upper and under-body for all models. 3-D effects from longitudinal vortices were not captured at the symmetry plane but are included in the base pressure since it covered part of the base area. The surface pressure in the symmetry plane is shown in Figure 35.

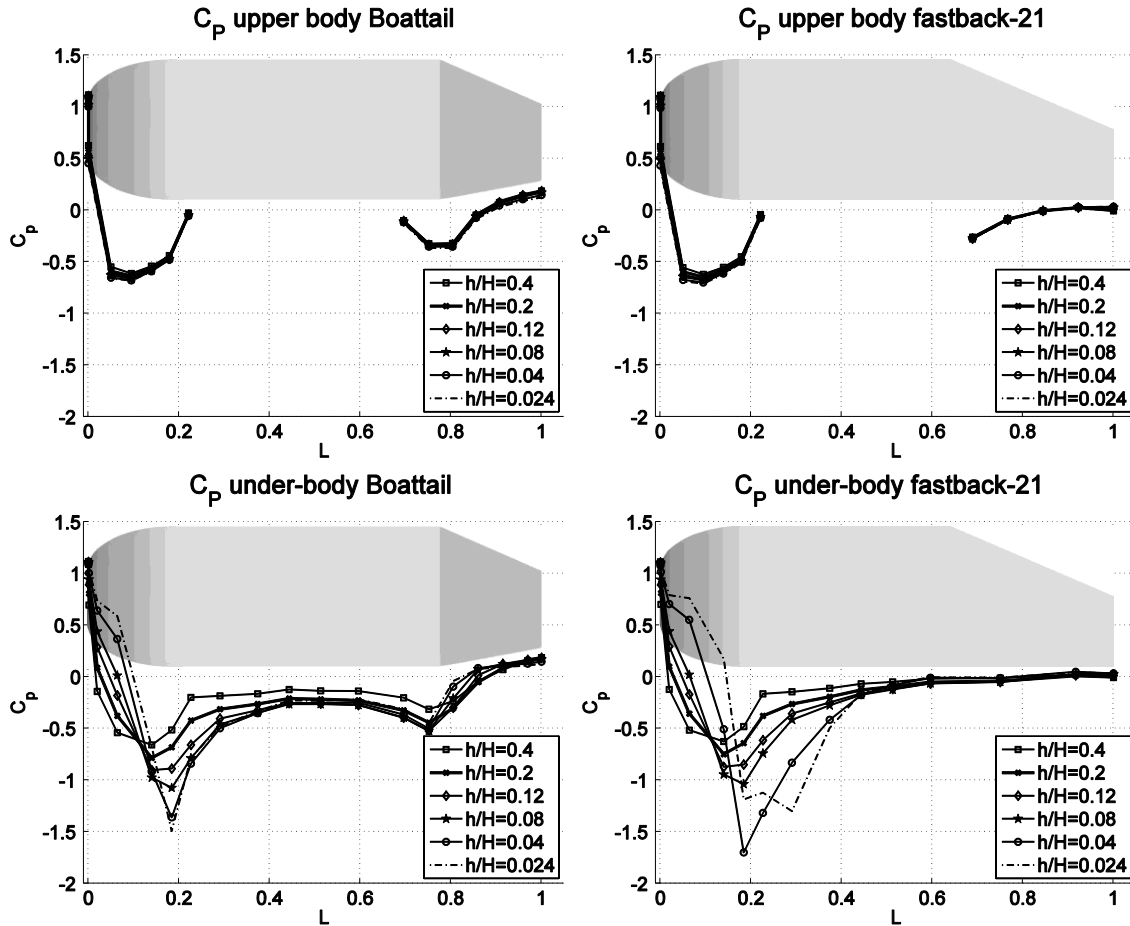


Figure 35 Surface pressure at symmetry plane from measurements.
Upper: Upper body pressure. Lower: Under-body pressure.

The variation of the average base pressure due to ground proximity is shown in Figure 36. The curves follow the inverted drag curve relative to ground proximity. Meaning that when the base pressure is increased, the drag is reduced and vice versa. The curves do not have the same shape between the different bodies since the ground effect changed the wake in different ways. When the Boat-tail had a reduced base pressure from increased ground proximity, the fastback21 had an increased base pressure. The boat-tail had an increased wake assymetry from reduced ground clearance due to the diffuser pumping effects. The fastback21 had better pressure recovery and smaller wake with reduced ground clearance. The drag of the body will also come from the projected area of the backlight. All models except the square-back had a backlight that was an additional part of the drag force.

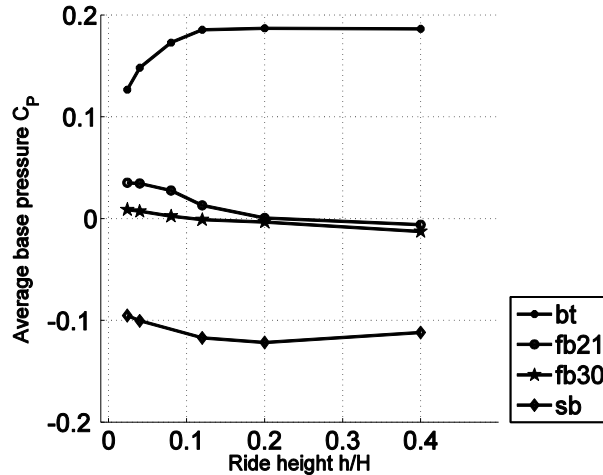


Figure 36 Average base pressure variation by ride height, with moving ground.

The surface pressure from the test data correlates well with result from simulations using the Chalmers wind tunnel domain as digital wind tunnel. In Figure 37 pressure of the symmetry plane, in the simulation extracted and plotted in matlab relative to test data, is shown for comparison. The curves for the boat-tail correlate well. The larger peaks at the start of the backlight and start of diffuser are related to the fact that the simulations provide pressure data with a very dense mesh, and the test result is limited to probe position. The distance between probe positions was between 40-60mm. There was a deviation at the last probe, of the front part, of the upper body for all the models. The radius at the front did not provide fully attached flow and the flow attachment was over-predicted in the simulations. The base pressure of the square-back was over-predicted in the simulation and is the reason that the drag of the model was under-predicted, as could be seen in Figure 27. Over prediction of the base pressure is related to the time average of the wake in the RANS since there was no critical separation angle. From the centre-line pressure of the upper body and under-body the results correlated well, except close to the base. As mentioned previously, the last point in the measurement was an average value of all the probes in the base. For the simulation it was only the surface pressure of the upper or under-body. The base pressure is compared in Figure 38 and the simulated results reveal an over-prediction for all models, but the difference was largest for the square-back. The results from the simulation are taken from identical probe locations as for the measurements. For the C_p , the dynamic pressure comes from the identical position as in the physical wind-tunnel. The boat-tail and the fastback21 used 10 probe positions each, and the square-back had 21 points. The result of the probe locations were extracted from the simulations and plotted in matlab.

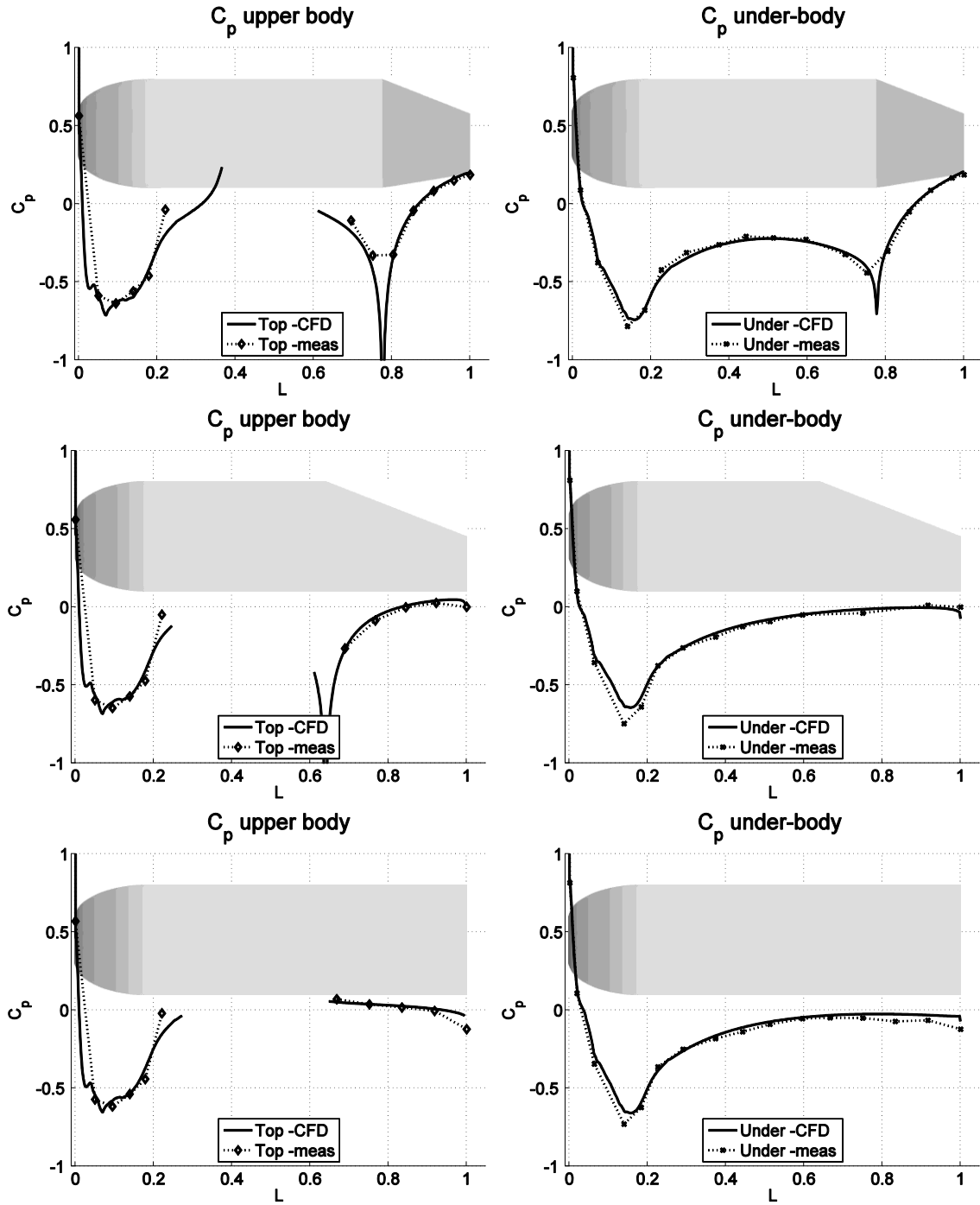
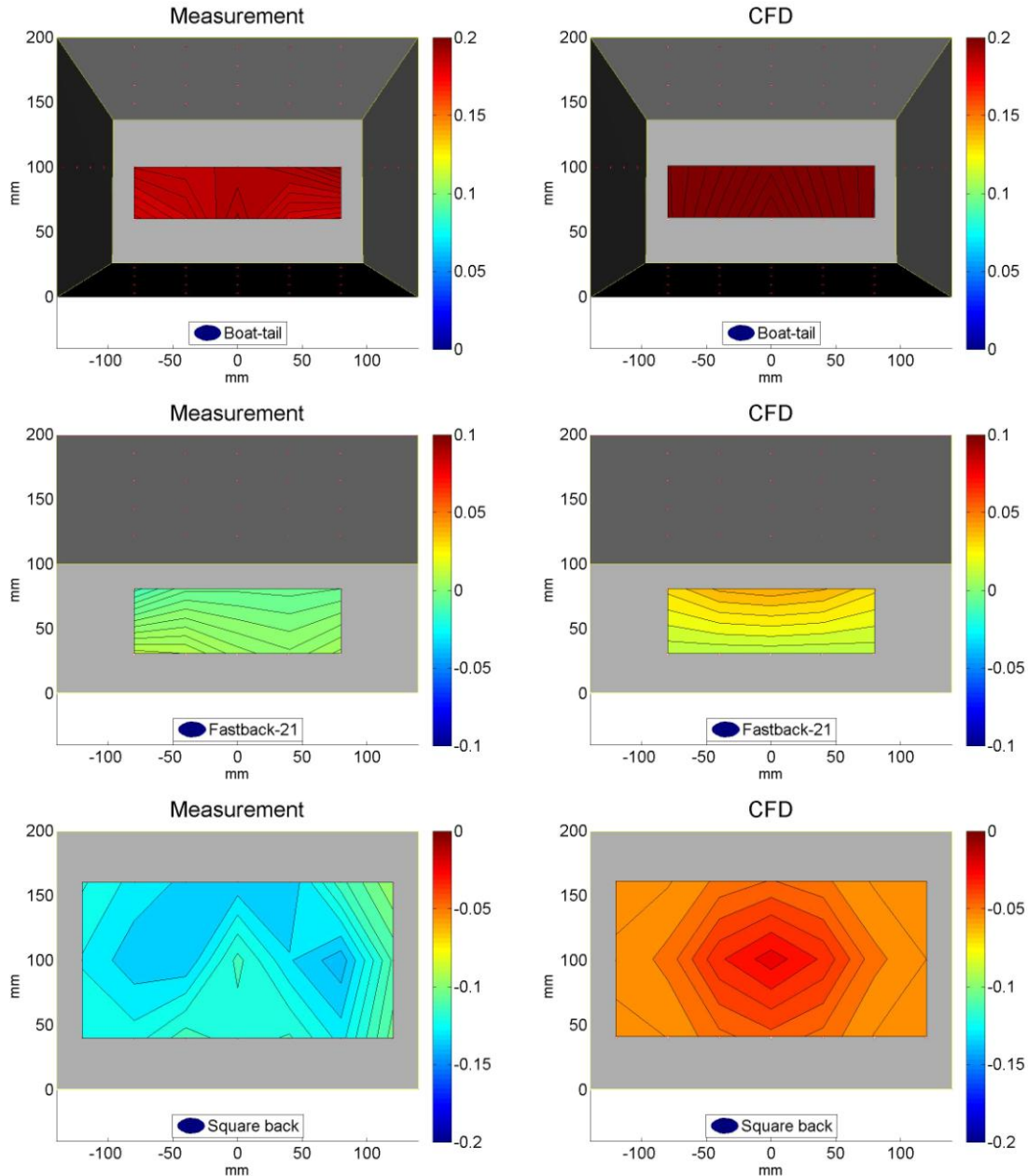


Figure 37 Surface pressure at symmetry plane from measurement and CFD simulation. From top to bottom: Boat-tail, Fastback21, Square back. Left: Upper body pressure. Lower: Under-body pressure.

The results from the simulations are symmetrical around the symmetry plane but the measurements include some asymmetry. This was due to the model in the wind tunnel having small geometric deviations in installation angles.



**Figure 38 Comparison of base pressure C_p from measurement and simulation
Left: Measurement. Right: CFD.**

Flow field from symmetry plane in CFD is presented in Figure 39. The model was fixed from the top and the sting was included in the simulation. The moving belt and boundary-layer suction plate is visible on the floor of the wind tunnel. The breather slot is included in the figures at the end of the test section as a 20 mm slot. It functions as a pressure equalisation in the test section and opened into the wind-tunnel laboratory hall. The left-hand pictures show the total pressure coefficients and the right-hand pictures show the velocity magnitude. Differences in size of the wake are evident and the asymmetric wake of the fastback21 indicates that it was blocking the under-body flow.

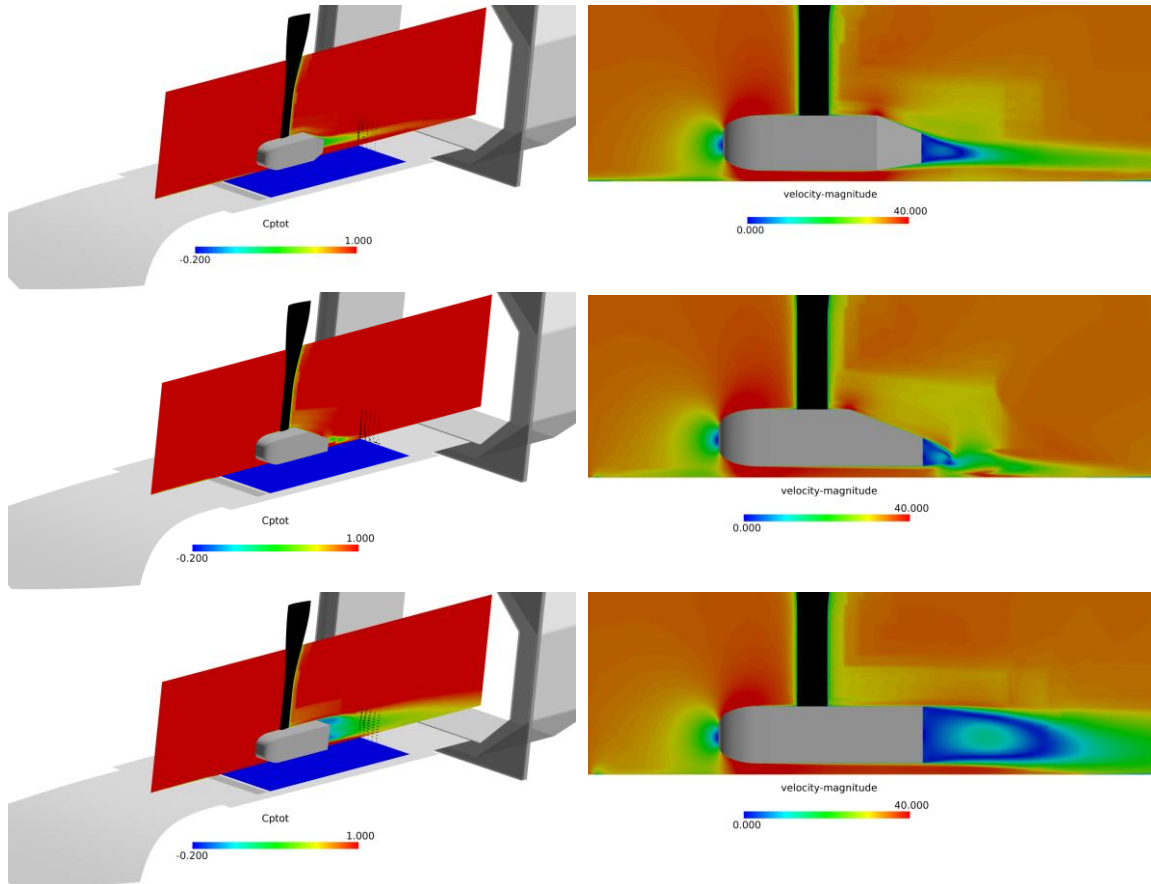


Figure 39 Flow field from CFD simulation with Chalmers wind tunnel domain as digital wind tunnel. Flow field in symmetry plane. From top to bottom: Boat-tail, Fastback21, Square back. Left: C_p of total pressure. Right: Velocity magnitude.

4.2. Passenger vehicle applications

The vehicle geometry was prepared to be identical with exception of the rear-end upper body. The same base geometry was used in paper I and paper II, but paper II had more detailed grid resolution. Front end, wheels, under-body, and engine compartment were the same and so were ride-height and pitch-angles. The wagon has a higher roof-line and thereby a larger frontal area. The taper angles at the rear were smaller for the wagon and the rear bumper was 20 mm longer for the wagon. This was all according to the actual geometry of the base vehicle according to their definition. The geometry was selected to exclude all geometry differences between vehicle types except for the upper body. The approach was to keep the benefit of bluff body aerodynamics, that is, well defined geometries, and combine the results with passenger-car geometries and boundary conditions. All the results from the vehicle simulations were carried out with moving ground, cooling flows and rotating wheels unless otherwise stated.

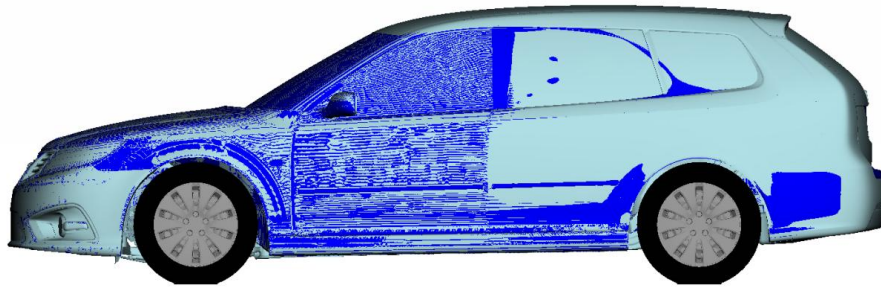


Figure 40 The sedan and wagon vehicle models overlaid. Only difference is at the rear end.

The flow around the vehicle was re-distributed depending on the rear-end shape. The notchback rear-end will accelerate the flow at the upper body and have a smaller wake. At the same time the flow at the under-body will be reduced and the wake flow is directed into the ground. Consequently there is a higher under-body flow of the wagon and a larger wake. Figure 41 shows the difference in velocity magnitude between a sedan and a wagon in symmetry plane. The red section is the higher air-speed in the downstream flow and blue shows the lower speed at the under body.

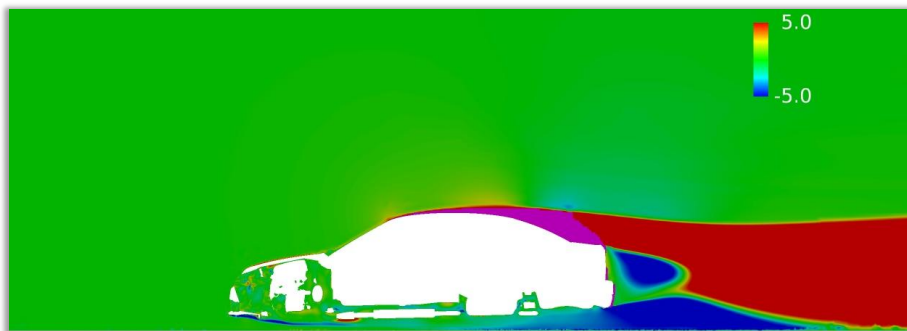
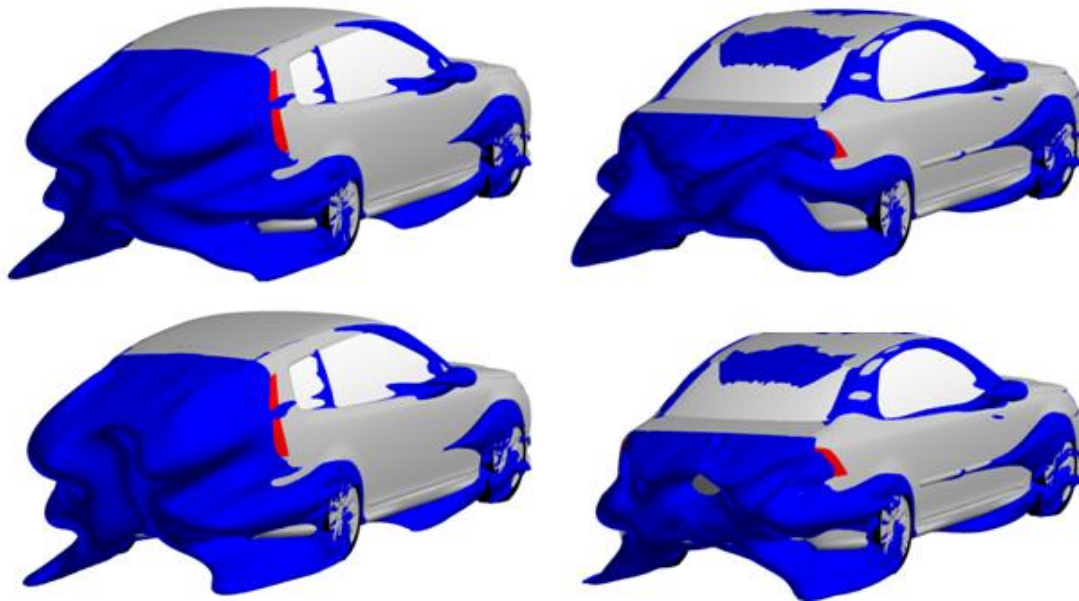


Figure 41 Difference in flow around sedan and wagon vehicle symmetry plane. Colour show relative velocity magnitude from wagon. Cyan colour is the cut out for the wagon body.

The cooling flow will change with different rear-ends due to the stagnation point at the front will be lower for the sedan. It was seen in this work that the sedan had slightly higher cooling flow relative to the wagon. To determine and extract the cooling drag is difficult but an accepted method is to measure the drag of the car with open and closed cooling-inlet, and extract the difference. This method will not only include the cooling system, since blocking the cooling inlet will generate flow re-distribution around the vehicle. The cooling drag will therefore be affected by vehicle type and rear-end shape. Another method, as proposed by Wiedemann et al., is to measure the momentum fluxes, and using conservation theorems [23] extract flow energy losses from cooling flow only. This is actually a more correct description of cooling drag by the cooling components, but more time-consuming measurements and higher complexity make the method less used in engineering. The cooling air of passenger cars is usually discharged to the under-body and wheel house for practical reason, and will generate some lift. Sports and race-cars have cooling outlets on the upper-side of the body for increased downforce or optimized cooling flow through the radiators.

The wake is significantly smaller for the sedan due to attached flow over the backlight that gave a smaller base area. The rear wheel wakes interacted with the base wake for both sedan and wagon rear-ends. Since a reduced drag comes from an increased base pressure, to a large extent, it is desirable to have attached flow as much as possible and reduce the separated region. Since the wheels and the wheel wake interacts with the base wake this will go hand in hand. The size of the separated region is reduced with a smooth under-body and a diffuser at the under-body. The upsweep generates a pressure recovery and guides the flow in an upward direction. The wake is represented by the iso-surface of the total pressure equal to 0 in Figure 42. It is clear that the base wake including wheel wake is reduced for the sedan. For the wagon the lower part of the centre is shorter and the wheel wakes are smaller with diffuser, though it is not so evident.



**Figure 42 Wake formations behind a sedan and a wagon vehicle from paper IV.
Upper: Reference vehicles. Lower: With under-body panel and diffuser.**

Drag reduction by reduced wake is achieved with a high pressure recovery at the rear end. When viewed from the side, angles such as backlight and under-body diffuser angles are important, but the plan view angles are also important. Taper angles of the rear-end generate a pressure recovery and reduce drag. Since the flow field around the wheel is highly turbulent, the flow behind the wheel is often separated from the body. This leads to the taper angles having no effect and producing no pressure recovery behind the wheel. A test carried out on a full-size clay model at FKFS wind tunnel by Saab automobile [36], resulted in no improvement in drag by increased taper angles behind the wheel. Figure 43 shows the test car and the location of tested taper angles. Successful pressure recovery requires flow to be attached to the body behind the wheel. A covered wheel will improve the possibility of attached flow behind the wheel, and enable a pressure recovery by a taper angle in the lower region.



Figure 43 Experiment carried out on a full size car at FKFS wind tunnel, by Saab Automobile.

Under-body covers with an under-body diffuser will reduce drag and lift of passenger cars, but the effect varies with upper body geometry. It is important to have undisturbed and attached upstream flow of the under-body. If the flow upstream of the diffuser has a thick boundary layer or is unattached to the floor, there will be very little or no pressure recovery over the length of the diffuser. An under-body cover with diffuser was applied to a Saab 9-3 car and tested on a sedan and wagon type for drag and lift effects. The simulated results are shown in Figure 44 as relative drag and lift from a reference car with non-flat floor. More information and details from the simulations can be found in paper II. Lift forces were significantly reduced and the reduction was larger for the sedan. Drag is reduced for the wagon with an optimum at 5 ° diffuser angle but drag reduction of the sedan was much higher. Optimum diffuser angle for the sedan was higher and approximately 8°.

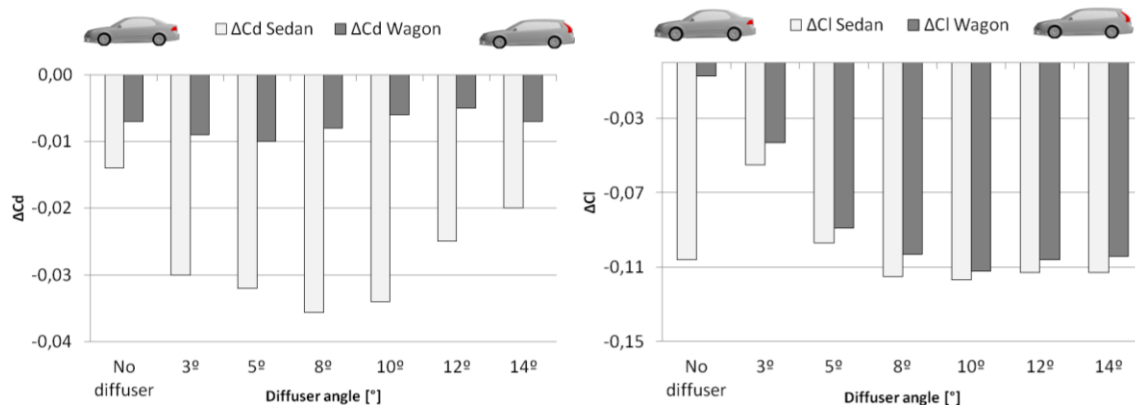


Figure 44 Reduced drag and lift by diffusers at sedan and wagon cars.

Drag reduction by an under-body diffuser is all about generating a pressure recovery to increase the base pressure. The panels including diffuser will increase the base pressure but the magnitude is not the same for the two body types. The pressure increase for the sedan is significantly higher and this is the reason for better drag reduction. The change relative to the reference car is made at the under-body but pressure recovery at the sides and trunk was also increased by the diffuser. Since the total size of the wake is reduced, as could be seen in Figure 42, the pressure also increases at the

sides. A plot of C_p of the sedan with 8° diffuser relative to the reference sedan, and wagon with 5° diffuser relative to the reference wagon is shown in Figure 45. For the wagon the effect of the base pressure was not of the same magnitude, and this followed the result of the drag reduction. The flow around the sedan will be cambered with the wake directed towards ground and the diffuser upsweep steering the flow to a more symmetric wake flow. The wagon already has a near symmetric wake flow so the upsweep enables a pressure recovery but it does not straighten the wake. This is the reason for the better drag reduction of the sedan. The sedan has higher lift than the wagon and this comes from the cambered flow, which is a result of the cambered shape of the body. The relation between drag and lift is parabolic, with a drag minimum relative to lift.

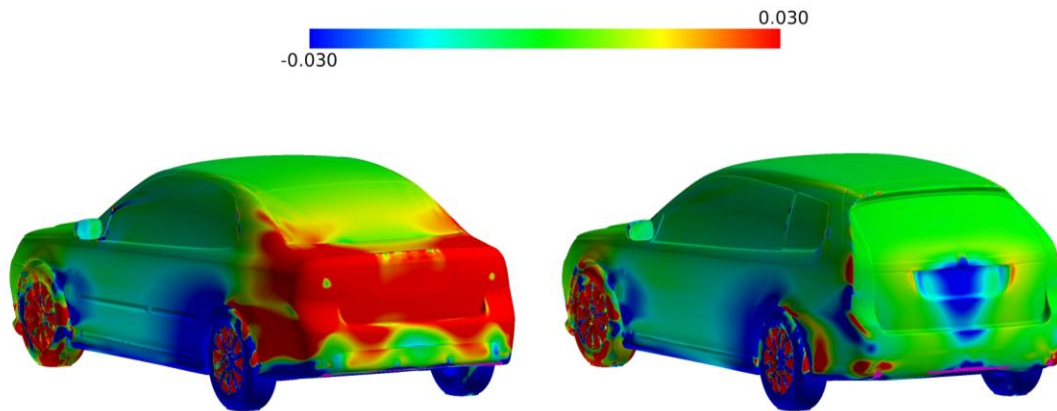


Figure 45 ΔC_p from reference vehicle. Left: Sedan. Right: Wagon [37].

The better pressure recovery from the diffuser of the sedan has to do with the symmetry of the wake. The flow around the sedan is cambered, in side view, and the wake flow is directed towards ground but for the wagon it is symmetrical for the reference vehicles. The diffuser generates a pressure recovery for both sedan and wagon, but for the sedan it also made the wake more symmetric. This combined effect is why the diffuser generates better drag reduction for the sedan. The sedan generates a significant amount of lift and the reference vehicle is far from optimum in the drag/lift curve discussed in Figure 6. A reduction of lift forces has a large impact on the drag. The wagon reference on the other hand is close to the optimum in the drag/lift ratio and has a smaller drag reduction by the diffuser. Lift increases until 10 degrees diffuser angle but the reduction then becomes smaller, for both vehicle types. There was a separation at the diffuser that no longer increased the under-body flow and reduced the under-body pressure. At full separation, the wake will start at the diffuser inlet and drag will thereafter be increased.

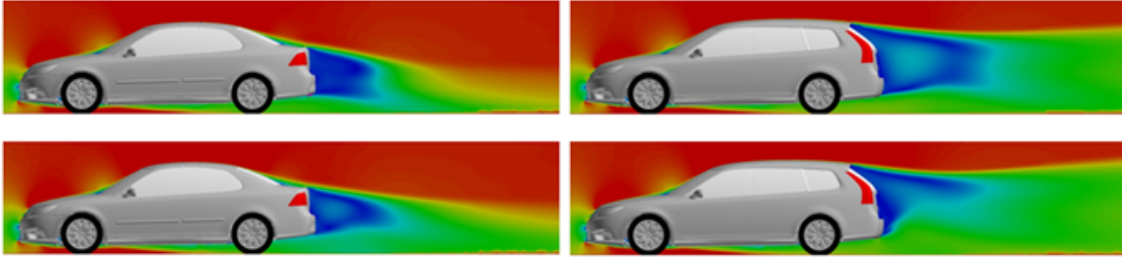


Figure 46 Velocity magnitude at symmetry plane for sedan and wagon vehicles.
Upper: Reference vehicle. **Lower:** With under-body cover and diffuser.

The pressure recovery at the diffuser varies over the width of the vehicle due to disturbed upstream flow. The panels do not cover the exhaust tunnel and there was turbulent flow from the wheels and from the cooling air. The variation in flow distribution was clear and the under-body pressure in four sections is shown in Figure 47. The flow in the outer sections is affected by the turbulence from the wheels, and the center section has more impact from the exhaust tunnel and cooling flows. The pressure recovery by the diffuser is relatively uniform, even if the flow in the outer section is partly blocked by components from the wheel suspension.

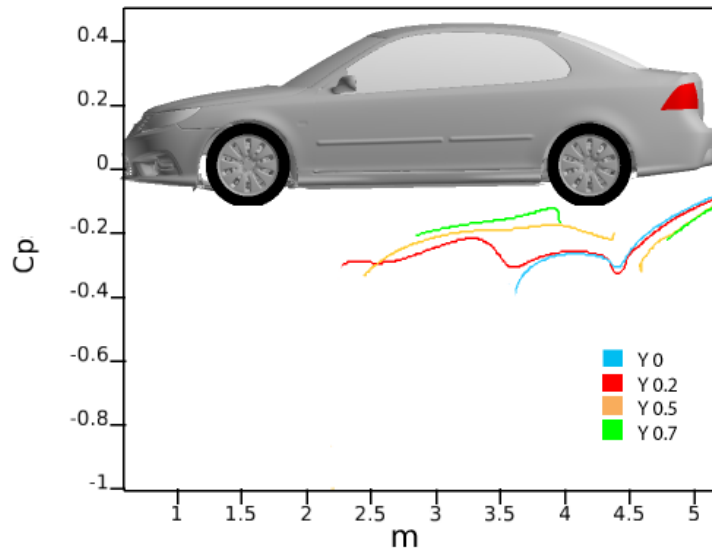


Figure 47 Under-body pressure of the sedan in four longitudinal sections.

An under-body diffuser requires attached flow to enable pressure recovery. A demonstration of this was made by removing the under-body covers and only retaining the diffuser itself. The surface pressure of the vehicle without under-body cover is shown in Figure 48 relative to the result of the vehicle with under-body cover. The importance of attached flow is visible and the base pressure recovery of the sedan is lost. The drag was higher than the reference vehicles, for the sedan $C_D +0.006$ and for the wagon $C_D +0.008$. The difference in base pressure was also here not as large for the wagon, but the diffuser itself had reduced pressure and the rearward projected area contributed to the drag increase.

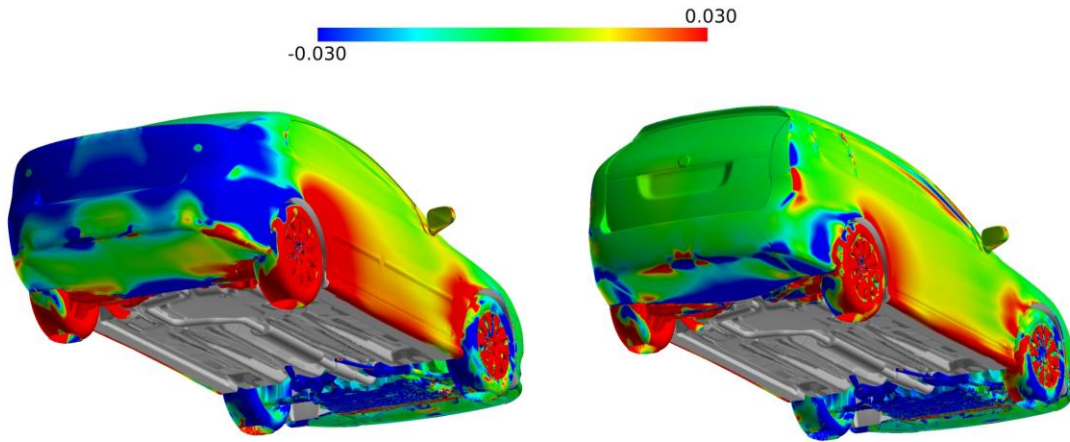


Figure 48 ΔC_p from best diffuser model to diffuser model without under-body cover. Sedan 8° diffuser, wagon 5° diffuser. Left: Sedan. Right: Wagon.

The cooling flow through radiator and engine bay is important for the drag of the car and for the under-body flow. Since the cooling air flow will exit at the under-body and wheel houses, it is important to predict this right for simulations of the under-body and diffuser flow. The full size reference car was tested in a wind tunnel with an anemometer rack mounted in the cooling module to determine the amount of flow going through the CRFM. The simulation reference model was tuned to have the same through-flow. Figure 49 show a illustration of the cooling flow, and how it will exit at the wheel houses and at the under-body. The cooling flow will have a major impact of the under-body flow and will eventually affect the wake.

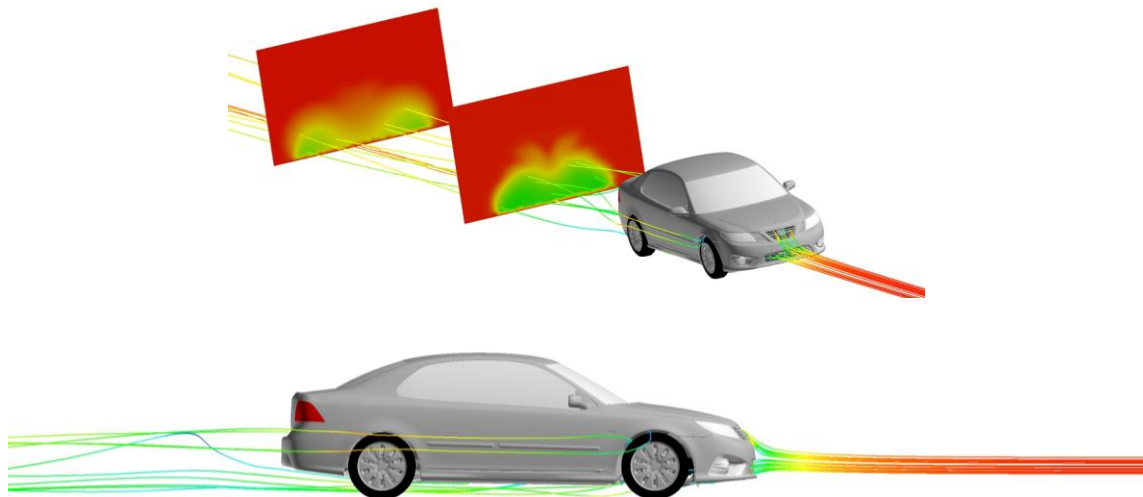


Figure 49 Streamlines to and from the cooling system coloured by velocity magnitude. Surface planes in wake flow also coloured by velocity magnitude.

The wagon vehicle has got higher under-body flow than the sedan due to the different rear ends. The under-body flow downstream of the front wheels is not uniformed due to the exit of the cooling flow. Adding smooth floor covers with diffuser increase the flow at the under-body, for both sedan and wagon, and generate an upsweep. Figure 50 is a plot of the under-body velocity magnitude; 0.1m above ground under the reference vehicles. Lower plot shows the relative difference in velocity magnitude when the diffuser is added. The wake is narrower for the wagon because the flow is directed more upward for the reference vehicle. Adding the diffuser to both models increases the upsweep of both models, but in total, the upsweep is stronger for the wagon. The plots make a clear view of the increased under-body flow due to the smoother under-body.

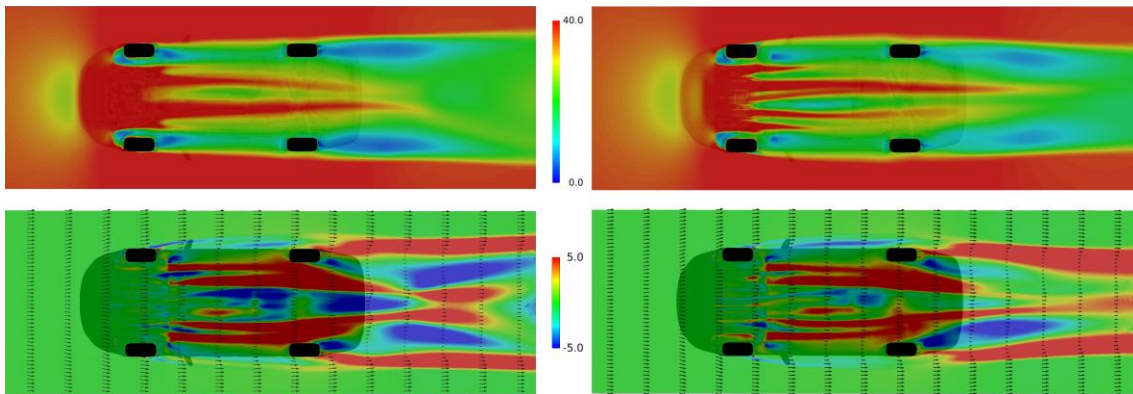
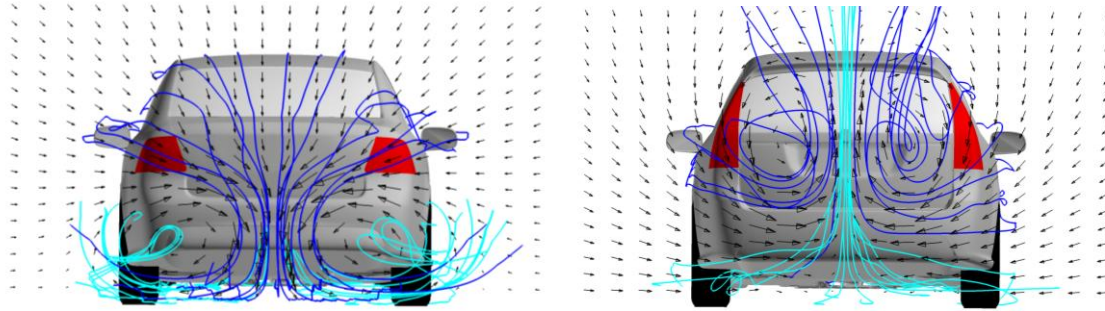


Figure 50 Under-body velocity magnitude of reference vehicles, upper. Relative velocity magnitude between reference vehicle and vehicle with under-body cover and diffuser, lower. Left: Sedan. Right: Wagon.

The sedan vehicle will have lift forces and the wagon car will have a down force after the panels and diffuser are added. The upper part of the flow generated longitudinal vortices that were directed down in the symmetry plane. The under-body generates vortices in the opposite direction, but the upper vortices were stronger and dominated further downstream in the wake. The wagon car generated the same vortices but the strength of the lower vortices were stronger and dominated. The result being vortices in the opposite direction relative to the sedan, further downstream. The flow around the sedan and wagon was cambered in opposite directions and thereby generated longitudinal vortices in opposite directions and of different heights from the ground. The longitudinal vortices are illustrated in Figure 51 by a vector plot 4 m behind the vehicles and streamlines released from the upper and under-body.



**Figure 51 Vortex vectors 4m behind sedan and wagon vehicles.
Streamlines released from upper body (dark) and from under-body (lighter).
Left: Sedan. Right: Wagon.**

Low pressure drag is achieved with the base wake as small as possible and the base area as small as possible. The best way to achieve is to enable maximum pressure recovery, and to do that a balanced wake is required. There is a drag minimum relative to lift forces and this is related to the balanced wake, and a minimum of vortex drag. This does not correlate with a symmetrical body since the ground will change the flow distribution above, and under, the vehicle and effectively change the camber of the body.

4.2.1 Energy usage

The power a vehicle requires for propulsion must be equal to all the driving resistance that the vehicle has to overcome, plus losses. The total driving resistance is described by equation (4). The ultimate goal with reducing the aerodynamic drag of a passenger car is to reduce the fuel consumption of the vehicle. To test the effect of reduced drag and measure the reduced fuel consumption for the customer, there are specified driving cycles defined. The NEDC (New European Driving Cycle) is specified on level roads and used in Europe. The cycle is approximately 11 km in length and the average speed is 33.6 km/h. Figure 10 is a plot of the driving speed relative time, including acceleration and idle times. Similar driving cycles are available in the U.S. defined by NHTSA and EPA.

The energy required to run the vehicle through the NEDC driving cycle was measured by simulating the driving cycles. This is an example of the energy saving by the reduced drag generated by the diffusers, in the vehicle propulsion phase. The result does not consider efficiency of driveline or any mechanical system but gives a quantitative energy requirement for the defined driving behaviour and vehicle speed. For the friction resistance, a constant friction coefficient of 0.01 is used and a gravity of 9.81 m/s². The sedan and wagon had different mass and frontal areas and the inputs are specified in **Table 4**. The reference C_D was the C_D of the reference vehicles in the simulations and the ΔC_D was the improvement for the best diffuser model.

Table 4 Data used in driving cycles

			Sedan	Wagon
Mass	m	[kg]	1600	1660
Front area	A	[m ²]	2.168	2.218
Gravity	g	[m/s ²]	9.81	9.81
Friction coefficient	fr	[-]	0.01	0.01
Drag coefficient	C _D	[-]	-	-
Delta drag coefficient	ΔC _D	[-]	-0.038	-0.009

The energy required to drive the vehicles around the driving cycles was simulated and the data was normalized with the result from the reference vehicle. The test cycle included accelerations, idle times, driving speeds, driving distance and speed. The required energy was the power required integrated over the time of the driving cycle, $E=P*t$. The power required is the resistance forces multiplied by vehicle speed $P=F_x*V$. The idling times was set to zero energy required as well as the deceleration. The energy saved by the under-body panels and diffuser is shown in Figure 52. The improvement for the sedan was approximately 4%, from 13 % reduction of the drag coefficient C_D. The relatively low energy saving from improved aerodynamics is due to the low average speed in the driving cycle. The total added mass of the under-body covers with diffuser will be very dependent on the individual design. The panels will add mass to the vehicle but the integration to the vehicle may end up in removal of components that reduces mass. Adding mass leads to increased energy usage for the vehicle in the test cycle due to additional acceleration and friction forces. An additional 30 kg added by the panels, approximately 1.8%, results in 1.2% loss in energy and would lead to a reduction of the total energy improvement to 3%. The same for the wagon shows that the total energy saved by the panels was 1% in the NEDC. If 30 kg was added by the under-body covers the improvement was lost. A linear adding of mass results in a near linear additional energy requirement in the driving cycle.

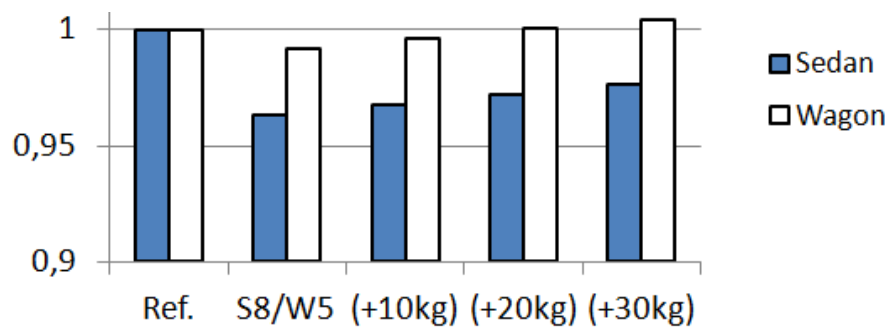


Figure 52 Energy required for the sedan and wagon vehicles to run the NEDC relative to energy required by the reference vehicles.

The aerodynamic drag has a relatively small effect in the NEDC due to a low average vehicle speed. In constant speed driving, at highway speeds and urban road driving speeds, the effect was larger. The power required to drive the sedan vehicle was reduced 9.5 % by the under-body panels, at 120 km/h; at 80 km/h it was a near 7% power

reduction. Also at constant speed driving an added mass had an impact of increased power required due to additional rolling resistance. The increased power required by 30 kg added mass was less than 0.5%. The added panels to the wagon resulted in reduced power consumption by 2.5% at 120 km/h and 1.8% at 80 km/h. An added mass of 30 kg still leads to a reduction of the engine power needed. The results are presented in Figure 53.

The effect of the aerodynamic drag is more noticeable at higher vehicle speed due to the square of velocity dependance of the aerodynamic drag force term, and the reduced impact of mass. Even though the reduced power for propulsion is large, this does not lead to the same magnitude of reduced fuel consumption. Reduction of fuel consumption will be dependent on the efficiency of the powertrain and driveline, idling power needed, and more rolling resistance. But it is clear that the more effective the powertrain and driveline is, the closer to this result it will be. Reduced power requirement means that the powertrain can be reduced, and this leads to the possibility to reduce mass of chassis and body. The weight spiral is an important factor.

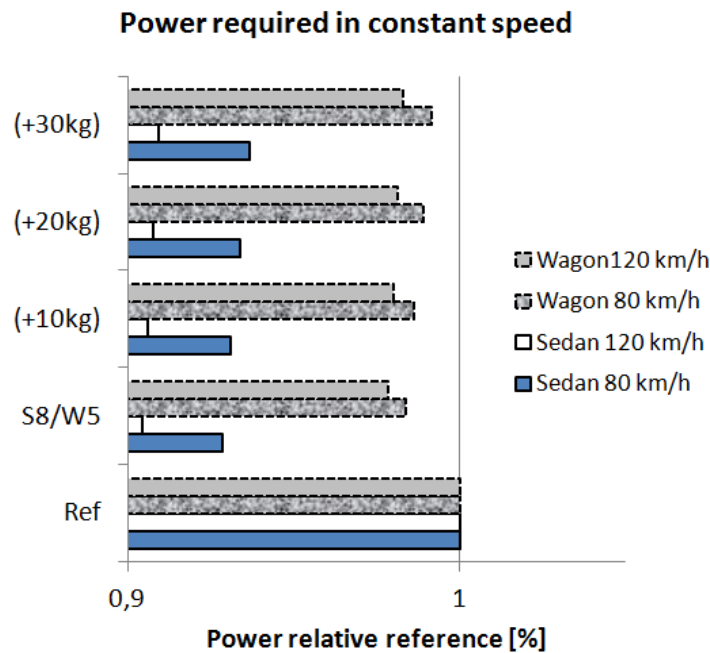


Figure 53 Power required for propelling the vehicles at constant speed driving relative to reference vehicles.

5. Concluding remarks

Passenger cars are bluff bodies aerodynamically, with the pressure drag dominating the friction drag. Reducing the pressure drag has the greatest potential and the focus should be at this. The exterior body of a passenger vehicle, such as the upper and under-body, is responsible for more than 60 % of the drag. The rest is related to cooling flows and wheels. It is therefore relevant to study the vehicle body alone, and do so with simplified models of vehicle proportions. Simplified bluff bodies were used to study the overall effects of the body shape with regard to ground proximity, ground simulation, yaw and pitch angles.

- The rear-end shape was seen to have a major effect on the flow distribution around the body. The effect of drag and lift dependence on ground proximity is very different depending on rear-end shape.
- A body of vehicle proportions will have reduced drag by a nose-down pitch as long as the flow does not generate a negative camber.
- There is an optimum drag relative pitch angle and yaw angle of a body.
- A square back model will have a larger drag increase by a yaw angle than other shapes.
- Drag reduction of an under-body diffuser, applied to a simplified bluff body is depending on the upper body. A model with large backlight angle will have better drag reduction by a diffuser than a square back model.
- Diffusers applied to passenger vehicles, with road vehicle boundary conditions, follow the same trend as diffusers applied to simplified bluff bodies. The main part of lift and drag of a passenger car is related to the main body.
- The sedan vehicle has greater potential to reduce drag by using a smooth floor and under-body diffuser than the wagon. The diffuser generates an upswEEP and makes the wake more symmetrical in side view, for the sedan. For the wagon the wake is already symmetrical and the diffuser can even generate an asymmetric wake.
- Wake symmetry is very important for optimum pressure recovery of passenger vehicles.
- The effect of correct ground simulation is shown to be important since the flow around the body will be re-distributed to have more flow under the body.

6. Future outlook

This work would benefit to have comparable measurement of full scale vehicles in a wind tunnel, for validation. A full scale test was planned but had to be cancelled due to the Saab Automobile bankruptcy. Another approach with the simulations is recommended. Conducting studies with transient simulations, and finer refinement of the boundary layer is out of interest. More detailed studies of the absolute agreement between measurement and simulation, especially for lift. Another recommendation is to extend the study of diffusers applied to passenger vehicles with test and simulations in yaw conditions. This would increase detail knowledge in diffuser function at real life operation.

7. Summary of papers

This chapter presents a brief summary of the papers appended to this thesis. The summary is a quick overview of the key findings and a description of the objective of the study.

Paper I.

Marklund J. Löfdahl L. Influence of a Diffuser To The Wake Flow of a Passenger Car, ASME Summer Meeting FESM2012, 8-12 July 2012, Rio Grande, Puerto Rico, USA.

Varying effect of a diffuser, depending on upper body, was found in bluff body experiments and the objective was to test this idea at full scale vehicles. The study was formed to test a diffuser applied to cars under road vehicle boundary conditions in CFD. The simulation models were setup to a sedan and a wagon car and tuned to road vehicle boundaries. The result was that there was a significant difference in the drag reduction improvement between the sedan and the wagon vehicle. The difference was seen to be related to the base pressure recovery and the wagon vehicle does not have the same potential as the sedan.

Paper II.

Marklund, J., Lofdahl, L., Danielsson, H. and Olsson, G., "Performance of an Automotive Under-Body Diffuser Applied to a Sedan and a Wagon Vehicle," *SAE Int. J. Passeng. Cars - Mech. Syst.* 6(1):2013, doi:10.4271/2013-01-0952.

This paper extends and expands the study in Paper I. More details and 3D effects were studied. Similar simulations were carried out with a more detailed computational grid. The better drag reduction potential of the sedan was confirmed and lift forces were shown to be reduced with increased diffuser angle. This is not valid for high diffuser angles due to flow separation. Changed flow distribution above and under the vehicle depending upper body, that is, higher under-body flow for wagon body. Also, an increased under-body flow due to the diffusers. Undisturbed upstream flow of the diffusers was shown important. The wheel wakes were shown to interact with the base wake and covered wheels reduces drag, also in combination with a diffuser.

Paper III.

Marklund, J., Lofdahl, L., “The Influence of Ground Proximity on the Flow Field around Different Bluff Bodies”, Submitted to Journal of Fluids Engineering.

This study was an extensive study of bluff body models with different rear end shapes and the effect of drag and lift. The study was both experimental and numerical where forces and surface pressures were compared. Simulations correlate well with measurements and the wind tunnel effects were seen to be very important. Different rear end shapes were seen to have a big variation in lift and drag depending on pitch-, yaw angles and ground proximity.

Paper IV.

Marklund, J., Lofdahl, L., “Effect of an Under-body Diffuser to the Aerodynamic Performance of Sedan and Wagon Type Cars”, Submitted to Journal of Fluids Engineering.

This paper compares the effects of a diffuser applied to a simplified bluff body and passenger vehicles. The drag reduction by the diffuser follows the same trend for the vehicles as for the simplified bodies. The drag reduction is relatively larger for the simplified bluff body compare to the passenger cars. Effects from the wheels and separated regions are only affected by the diffuser to a small extent. The result from this is that the full potential of the diffuser is bigger on the simplified body.

8. References

- [1] OICA International Organization of Motor Vehicle Manufacturers, <http://oica.net/category/production-statistics> available on 2013-03-23
- [2] ACEA, Association des Constructeurs Europeens d'Automobiles, http://www.acea.be/images/uploads/files/ACEA_POCKET_GUIDE_2012_UPDATED.pdf
- [3] BP statistical review of world energy, proven oil reserves. http://www.bp.com/assets/bp_internet/globalbp/globalbp_uk_english/reports_and_publications/statistical_energy_review_2011/STAGING/local_assets/pdf/statistical_review_of_world_energy_full_report_2012.pdf available on 2013-03-23.
- [4] Exxon, Energy outlook, http://www.exxonmobil.com/Corporate/energy_outlook_dm.aspx, available 2013-03-27
- [5] Oilprice.com, <http://oilprice.com/Energy/Energy-General/10-Interesting-Energy-Statistics-from-2012.html> available at 2013-03-26.
- [6] Elways, <http://elways.se/batteri-eller-direktmatning/>, available 2013-04-02.
- [7] Svenska Petroleum & biodrivmedel institutet, <http://spbi.se/blog/faktadatabas/artiklar/berakningsmodeller/> available 2013-04-02.
- [8] Tesla motor, <http://www.teslamotors.com/roadster/specs#specs-2>
- [9] EEC Directive 90/C81/01. www.dieselnet.com/standards/cycles/ece_eudc.phb
- [10] Tritton, D J., Physical Fluid Dynamics, Second Edition, ISBN 0 19 854493 6, OXFORD, 1998
- [11] Euro motor lecture series, FKFS, Wiedemann J. September 24-28, 2007, Stuttgart, Germany
- [12] Schlichting, H., Boundary Layer Theory, Sixth Edition, McGraw Hill, ISBN 07-055329, 1968.
- [13] Barnard R H, Road Vehicle Aerodynamic Design, Second edition, 2001, ISBN 0-9540734-0-1.
- [14] Marklund J., Minimize Vortex Drag of a Passenger Car, Licentiate thesis Chalmers University of Technology, Gothenburg, Sweden, 2010.
- [15] Howell Jeff, The effect of Back Light Aspect Ratio on Vortex and Base Drag for a Simple Car-Like Shape, SAE 2008-01-0737, Detroit, Michigan, April 14-17, 2008.
- [16] Howell Jeff, Le Good Geoff, Vortex Drag for a Simple Bluff Body at Incidence in Ground Proximity, Detroit, Michigan, April 11-14, 2005.
- [17] Wickern, G., Wagner, A., Zoerner, C., ,Induced Drag of Ground Vehicles and Its Interaction with Ground Simulation, SAE 2005-01-0872, Detroit, Michigan, April 11-14, 2005.
- [18] Howell Jeff, Haynes Trevor, The Influence of Lift on the Underbody Drag for Cars, 7th MIRA International Vehicle Conference, 22-23 October, 2008.
- [19] REGULATION (EC) No **443/2009** OF THE EUROPEAN PARLIAMENT AND OF THE COUNCIL of 23 April 2009 <http://eur-lex.europa.eu/LexUriServ/LexUriServ.do?uri=OJ:L:2009:140:0001:0015:EN:PDF>
- [20] Auto electronics, http://autoelectronics.com/powertrain/electrical_power_systems/regenerative-braking-free-0501/, available 2013-04-03
- [21] Hucho, W H. Aerodynamics of Road Vehicles, Society of Automotive Engineers, Inc. USA, 1998
- [22] Landström Christoffer, Flow field investigation of rotating wheels on passenger cars, Ph.D. Thesis, Department of Applied Mechanics, Chalmers university of Technology, 2011.
- [23] Hucho W H. Aerodynamik des Automobils, Friedr. Vieweg & Sohn Verlag/GWV Fachverlage GmbH, Wiesbaden, Deutschland, 2005.
- [24] Presentation_aerolab_BMW_group <https://www.press.bmwgroup.com/pressclub/p/me/download.html?textId=54913&textAttachmentId=72973> Available 13-04-22
- [25] Kevin R. Cooper, T.Bertenyi, G. Dutil, J.Syms. The Aerodynamic Performance of Automotive Underbody Diffusers. SAE 980030. Detroit, Michigan, February 23-26, 1998.
- [26] Panton, Ronald L. *Incompressible Flow*, John Wiley and Sons, Inc. NY, U.S.A. 1996.
- [27] Schutz T., CFD Analysis of Submerged Air Inlets for Automotive Applications, 8 FKFS Conference, Stuttgart, Germany, October 5-6, 2011.
- [28] Onorato, M., Drag Measurement Through Wake Analysis, SAE 840302. Detroit, Michigan, Society of Automotive Engineers, 1984.
- [29] Hackett, J.E., Sugavanam, A., Evaluation of a Complete Wake Integral for the Drag of a Car-Like Shape, SAE paper No.840577, Detroit, Michigan, Society of Automotive Engineers, 1984.

- [30] Cogotti, A., Flow Field Surveys Behind Three Squareback Car Models Using a New Fourteen-Hole Probe, SAE870243, Society of Automotive Engineers, Warrendale, 1987.
- [31] Cogotti, A., A Strategy for Optimum Surveys of Passenger-Car Flow-Fields, SAE890374, Society of Automotive Engineers, Warrendale, 1987.
- [32] Specification of rapid prototyping equipment from Saab Engineering services available 2012-11-05 <http://www.saabengineering.com/prototyping/model-manufacturing-and-rapid-prototyping/rapid-prototyping/>
- [33] Fluent Inc. (2009): ANSYS/*Fluent 12.0 User's Guide*, Fluent Inc. Lebanon
- [34] Hucho, W H., Aerodynamik der Stumpfen Körper, ISBN 978-3-8348-1462-3, Deutschland, 2002
- [35] Ahmed, S.R. Ramm, G, Some Sailable Features of the Time- Averaged Ground Vehicle Wake, SAE 840300
- [36] Ahlström, C. Test of aerodynamic features, Report from the new Saab 9-3 program, Saab Automobile 2009.
- [37] Marklund, J., Lofdahl, L., Danielsson, H. and Olsson, G., "Performance of an Automotive Under-Body Diffuser Applied to a Sedan and a Wagon Vehicle," SAE Int. J. Passeng. Cars - Mech. Syst. 6(1):2013, doi:10.4271/2013-01-0952.